VOLUME 19 NO. 1 |JANUARY 2025
P-ISSN: 1411-1616 | E-ISSN:2549-8215

JURNAL ILMIAH BERKALA SAINS DAN TERAPAN KIMIA

Natural Antique Vase Red (Suprabanindya *et al*, p. 20)

JURNAL ILMIAH BERKALA
SAINS DAN TERAPAN
KIMIA

PUBLISHED BY:
CHEMISTRY DEPARTMENT, FACULTY OF MATHEMATICS AND NATURAL SCIENCES
LAMBUNG MANGKURAT UNIVERSITY, INDONESIA

Jurnal Ilmiah Berkala: Sains dan Terapan Kimia
Vol. 19 No. 1, January 2025

SUPERVISORY BOARD

Head of Chemistry Department, Faculty of Mathematics and Natural Sciences, Lambung Mangkurat University

PUBLISHER

Chemistry Department, Faculty of Mathematics and Natural Sciences, Lambung Mangkurat University

MAILING ADDRESS

Jl. A. Yani Km. 36 Banjarbaru, Kalimantan Selatan , Indonesia 70714
Phone: 0511-4773112, 0511-4782899
Email: jstk@ulm.ac.id

FIRST EDITION: 2007

EDITOR IN CHIEF

Dahlena Ariyani, S.Si., M.S.

EDITORIAL BOARD

Associate Editors : Dyah Ayu Pramoda Wardani, M.Sc.
Section Editors : Achmad Ramadhanna'il Rasjava, S.Si., M.Si.

Editorial Board Members:

Prof. Dr. Abdullah, S.Si, M.Si (Universitas Lambung Mangkurat, Banjarbaru)
Prof. Dr. Gusrizal, S.Si., M.Si. (Universitas Tanjungpura, Pontianak)
Prof. Dr. Rer.nat Drs. Karna Wijaya, M.Eng (UGM, Yogyakarta)
Prof. Sunardi, S.Si., M.Sc., Ph.D. (Universitas Lambung Mangkurat, Banjarbaru)
Dr. RR. Dirgarini Julia Nurlianti Subagyono (Universitas Mulawarman, Samarinda)
Sura Menda Ginting, Ph.D. (Universitas Bengkulu, Bengkulu)
Yuana Nurulita,S.Si, M.Si, Ph.D (Universitas Riau, Riau)
Achmad Ramadhanna'il Rasjava, S.Si., M.Si. (Universitas Lambung Mangkurat)
Dahlena Ariyani, S.Si., M.S. (Universitas Lambung Mangkurat)
Dyah Ayu Pramoda Wardani, M.Sc. (Universitas Lambung Mangkurat)

SITE EDITOR AND ADMINISTRATOR

Dyah Ayu Pramoda Wardani, M.Sc.
Achmad Ramadhanna'il Rasjava, S.Si., M.Si.
Aulia Rhamdani Arfan, S.Si., M.Si.

ABOUT US

(Jurnal Ilmiah Berkala) Sains dan Terapan Kimia publishes scientific articles in the Chemistry field which include, but not limited to, research in chemistry, theoretical chemistry, and applied chemistry. This journal also publishes review articles about the development of chemistry. All the articles in this journal will go through a peer-review process to ensure that the quality of the article meets our standard before being published. Each article submitted to our journal will be reviewed by a reviewer having the expertise in the field. Shall the article submitted is deemed acceptable to be published in our journal, it is the writer's responsibility to make the necessary change and revision as recommended by the reviewer.

This journal is open access journal which means that all content is freely available without charge to users or / institution. Users are allowed to read, download, copy, distribute, print, search, or link to full text articles in this journal without asking prior permission from the publisher or author.

Sains dan Terapan Kimia (Jurnal Ilmiah Berkala) is published twice a year on January and July. There is no fee for authors to submit their manuscripts to be considered for publication in this jurnal. When the article is accepted for the publication. The publication fee is IDR 350.000,00 that covers article processing and DOI processing charge. Payment should be made by bank transfer to this account below

Bank : BNI Banjarbaru
Account Number **107840008**
Account Name : Dahlena Ariyani

Please send a confirmation of your proof of payment to jstk@ulm.ac.id

TABLE OF CONTENTS

Green Synthesis of CaO Nanoparticles from Chicken Eggshell using Lemongrass Leaf Water Extract.....1-9
Gladys Ayu Paramita Kusumah Wardhani and Nina Ariesta

Application of Palm Solid Waste Ash as A Ceramic Glazing Material.....10-24
Caecilia Tridjata Suprabanindya, Himawan Tri Bayu Murti Petrus, Fariz Al Hazmi

The Potential of Ironwood as an Activated Carbon Adsorbent for Heavy Metal Mercury (Hg) using the Pyrolysis Method.....25-36
Zimon Pereiz, Chuchita, Efriyana Oksal, Miranti Maya Sylvani, Ahmad Irawan, Yunus Pebriyanto, Ruslianannur Hairiah, Arini Eka Jaya Prastiti, Caroline Berlisnora Dasilva, Violina Anatasya, Risky Prisnanda

Synthesis And Characterization Of Acid-Activated Sago Dregs Biochar And Testing Its Ability As An Adsorbent For Rhodamine B Dyes.....37-51
Musa Habib, Dahlena Ariyani, Ahmad Budi Junaidi

Ethanol Extract of Areca Nut (*Areca catechu* L.) as a Complexing Agent to Determinate Fe(III) in Aqueous Medium..... 52-59
Pius Dore Ola, Dodi Darmakusumah, Luther Kadang, Suwari, Tabita Rihi and Yustina Menge Tibo

JURNAL ILMIAH BERKALA SAINS DAN TERAPAN KIMIA

Jurnal Ilmiah Berkala: Sains dan Terapan Kimia
Vol. 19 No. 1, Januari 2025

Green Synthesis of CaO Nanoparticles from Chicken Eggshell using Lemongrass Leaf Water Extract

Sintesis Hijau CaO dari Cangkang Telur Ayam Menggunakan Ekstrak Air Daun Sereh

Gladys Ayu Paramita Kusumah Wardhani[1*] and Nina Ariesta[2]

[1,2]Chemistry Department, FMIPA, Universitas Nusa Bangsa, Jl.KH Sholeh Iskandar Km 4, Cibadak, Tanah Sareal, Bogor, West Java, Indonesia - 16166

Email: *gladys.paramita@gmail.com, naariesta@gmail.com*

ABSTRACT

Sources of CaO in the synthesis of nanoparticles can be available from waste such as eggshell waste which has an average $CaCO_3$ content of 94%. This study aimed to synthesize nanoparticles with various compositions of CaO-0 and CaO-1 (50:50) derived from chicken eggshells, mediated by Cymbopogon citratus leaf extract, and to characterize the nanoparticles. Based on the results of phytochemical screening, *C. citratus* extract contained alkaloids, flavonoids, triterpenoids, and tannins. The results of characterization with UV-Vis spectrophotometer showed that CaO was formed at the highest wavelength with a composition of CaO-1 (50:50) with a value of 250-300 nm. Absorption band of FT-IR spectra at wave numbers 428 cm^{-1} and 711 cm^{-1} indicated Ca-O vibrational band and Ca-O bonds, respectively. The particle size of crystalline CaO-0 based on calculations using the Debye Scherrer formula ranged from 33.72 - 38.48 nm while the particle size of crystalline CaO-1 ranged from 28.93 - 70.75 nm with diposide and calcite phases based on XRD data. The surface morphology using SEM showed that CaO-0 was shaped like an irregular cube while CaO-1 forms irregular spherical lumps.

Keywords: CaO, green synthesis, *Cymbopogon citratus*, nanoparticles.

Received: 23 November 2023 ; **Accepted**: 30 December 2024: **Available online**: 30 January 2025

1. INTRODUCTION

Alkaline earth metal oxide, calcium oxide (CaO), is an inorganic metal oxide that can be made in the form of nanoparticles. CaO for nanoparticle synthesis can be sourced from inexpensive and readily available waste, such as eggshell waste, fish scales, clam shell residues, and animal bones. Chicken eggshell is an abundant waste in Indonesia. In addition to coming from egg consumption waste by the community, eggshell waste is also produced by the chicken hatchery industry. The chemical composition of the egg shell is 94% $CaCO_3$, 1% $MgCO_3$, 1% $CaPO_4$, and the rest is organic material as much as 4% by weight of the egg shell (Stadelman, 2015). Calcium carbonate is the main composition in chicken eggshells which naturally forms calcite (Laca et al., 2017). Research conducted by Goli & Sahu (2018), reported that calcined eggshell powder contained 97.86 % CaO, 0.785 %

MgO, 0.387 % P_2O_5, and the rest was in the form of other metal oxides. CaO nanoparticles are interesting to research and develop because of their adsorption ability, catalytic activity, optical and electronic properties, antibacterial properties, and their ability as a drug delivery agent.

Nanoparticles can be synthesized by conventional chemical and physical methods. The disadvantage of the chemical method is that it requires a lot of reagents that are harmful and toxic to the environment, while the physical method requires a lot of energy and conditioning under controlled pressure (Kumar et al., 2019). Therefore, in recent years, plant-mediated nanoparticles synthesis has become increasingly important because it is simple and environmentally friendly. This kind of synthesis is known as green synthesis or biosynthesis (Marquis et al., 2016). Extracts from plants can act as both reducing and capping agents in the synthesis of nanoparticles. Iravani (2011) reported that this green synthesis process involves metal ions combining to form precursor building blocks which then self-assemble into nanoparticles. Based on this method, several metal nanoparticles such as Au, Ag, Pd, Pt, ZnO, and Fe have been successfully synthesized (Ain & Nor, 2013; Fatimah et al., 2020; Maringgal et al., 2020). Several studies believe that the presence of phytochemicals such as alkaloids, saponins, terpenoids, and tannins are involved in the synthesis of these nanoparticles (Poinern & Fawcett, 2019). CaO nanoparticles can be synthesized using plant extracts (Maringgal et al., 2020). The reducing properties of several different plant species play an important role in reducing Ca salts to CaO nanoparticles. Several biomolecules in plant extracts such as proteins/enzymes, vitamins, alcohol group compounds, polysaccharides, alkaloids, polyphenols, and other secondary metabolite compounds are involved in the bioreduction, formation and stabilization of metal nanoparticles.

CaO nanoparticles have been successfully synthesized using deionized water (DI water) solvent extract from Piper betel leaves, Trigona sp. honey, light green stems of *Cissus quadrangularis*, *Rhododendron arboretum* leaves, papaya leaves, green tea leaves, and *Ocimum sanctum* leaf extracts. (Anantharaman & George, 2016; Gurav et al., 2020; Maringgal et al., 2020; Marquis et al., 2016; Ramola & Joshi, 2019; Yoonus et al., 2020). One of the nanoparticles that can be synthesized through plant extracts is CaO nanoparticles. The plant extract that can be used is *Cymbopogon citratus* leaf extract. The *C. citratus* (lemongrass leaf) is also a plant that has the potential to be used as a mediation for the synthesis of nanoparticles because of its phytochemical compounds. The aqueous extract of *C. citratus* leaves, among others, contains flavonoid and phenolic compounds (Balakrishnan et al., 2014). The *C. citratus* is an Angiosperm plant that has been used to synthesize gold nanoparticles and act as a reducing agent (Smitha et al., 2020). The *C. citratus* as a reducing agent in the synthesis of CaO nanoparticles has never been reported. In this study, CaO nanoparticles were synthesized from chicken eggshells and mediated by *C. citratus* leaf extract.

2. MATERIALS AND METHODS

2.1. Materials

The materials used in this research are chicken eggshells from chicken hatchery in Caringin, West Java, *C. citratus* leaf (from Bogor, West Java), deionized water (Hanna), HCl (Merck), NaOH (Merck), $CaCl_2$ (Merck), universal pH indicator, and Whatmann 41 filter paper. The instruments used in this research are spectrophotometer UV-Vis (Bell Photomic UV-51), spectrometer Fourier Transform Infra-Red / FTIR (Shimadzu), X-Ray Diffraction / XRD (Shimadzu), Scanning Electron Microscope / SEM (Bruker).

2.2. Preparation of chicken eggshells into $CaCl_2$

Chicken eggshells are taken as waste from the chicken hatchery industry in the Caringin area, Bogor Regency, West Java. The eggshells were washed using warm distilled water until clean, then dried in an oven at 110 ^oC for 3 hours. After drying, the eggshells were mashed into a powder measuring 100 mesh. Egg shell powder is converted into $CaCl_2$ by adding 12.5 grams of chicken egg shell

powder to 250 mL of 1 M HCl and stirring using a magnetic stirrer until $CaCl_2$ is formed (Habte et al., 2019).

2.3. Preparation of CaO from chicken eggshell

$CaCl_2$ solution was added with 1 N NaOH drop by drop while stirring using a magnetic stirrer for 2 hours at a temperature of 60 ℃. The addition of NaOH was stopped until pH 12 and a precipitate formed in the solution. After 2 hours, the mixture was allowed to stand at room temperature for 3 - 5 days (cured) until the filtrate and precipitate separated. The precipitate was filtered using Whatmann No.41 filter paper and washed with deionized water. The precipitate obtained was then dried in an oven at 90 ℃ for 1 hour (Bano & Pillai, 2020). The weight of the precipitate which has stabilized is then calcined at 700 ℃ for 3 hours. CaO obtained was coded CaO-0. After calcination, the precipitate was cooled to room temperature and pulverized to become CaO powder. The CaO powder was then characterized for its structure and surface.

2.4. Preparation of C. citratus (Lemongrass) water extract

Fresh lemongrass leaves are washed with distilled water until clean and cut into small pieces. Lemongrass leaves are dried and crushed. The lemongrass leaf powder weighed as much as 50 grams and added with 100 mL of deionized water. This mixture was heated at 100 ℃ for 1 hour. After 1 hour, cooled down to room temperature. The mixture was then filtered using Whatmann filter paper. The filtrate obtained is lemongrass leaf extract which will be used in the synthesis of CaO nanoparticles. Lemongrass leaf extract was tested qualitatively for phytochemicals (phytochemical screening) according to the AOAC method (AOAC, 1990) include alkaloids, saponins, tannins, phenols, and flavonoids.

2.5. CaO synthesis using lemongrass leaf water extract

Lemongrass leaf extract and $CaCl_2$ with composition 1 = 50:50 v/v, the solution was stirred for 2 hours at 60 ℃. 20 mL of 1 N NaOH was added dropwise during stirring to pH 12 and a precipitate was formed. After 2 hours, the mixture was allowed to stand at room temperature for 3-5 days (cured) until the filtration and precipitate separated. The precipitate was filtered using Whatmann No.41 filter paper and washed with deionized water. The precipitate obtained was then dried in an oven at 90 ℃ for 1 hour (Bano & Pillai, 2020). The weight stabilized precipitate was then calcined at 700 ℃ for 3 hours. CaO obtained was coded CaO-1. After calcination, the precipitate was cooled to room temperature and pulverized to become CaO powder. The CaO powder was then characterized for its structure and surface.

2.6. Characterization of CaO nanoparticles

The *C. citratus* leaf extract, CaO-0 and CaO-1 solutions were characterized using a UV-Vis spectrophotometer at a wavelength of 200 - 600 nm to determine the maximum wavelength. CaO-0 and CaO-1 powders were characterized using spectrometer FT-IR with KBR pellet method at wave number 400 – 4000 cm^{-1}. CaO-0 and CaO-1 powders were characterized using XRD and SEM-EDX. Characterization of the structure, phase and determination of the crystal size of nanoparticles using XRD at an angle of 2θ 10 – 80° while the determination of the surface structure and particle size was carried out using SEM-EDX.

3. RESULTS AND DISCUSSION

3.1. C. citratus extracts phytochemical content

The *C. citratus* was extracted using DI water by a maceration method. Maceration method is an effective and simple method for the extraction of bioactive compounds in plant extracts (Ćujić et al., 2016). The *C. citratus* was extracted using deionized water (DI Water) by the maceration method. The results of phytochemical screening of *C. citratus* extract are shown in **Table 1**.

Table 1. Phytochemical screening test results

No.	Compound Group	Result
1	Alkaloid:	
	a. Dragendorf	-
	b. Mayer	-
	c. Wagner	+++
2	Flavonoid	+++
3	Saponin	+
4	Steroid/Triterpenoid	+++
5	Tanin	+++

Explanation:
(-) : Negative
(+) : Weak positive
(++) : Positive
(+++) : Strong positive

Based on the results of phytochemical screening, *C. citratus* extract contains alkaloids, flavonoids, triterpenoids, and tannins. This is in accordance with the research of Shah et al. which contains secondary metabolites in *C. citratus* in the form of triterpenoid, phenolic, and flavonoid compounds (Shah, et al., 2011). While Umar, et al. (2016) found alkaloid compounds, tannins, and alkaloids in the extract of *C. citratus*. These secondary metabolites have a role in the synthesis of CaO nanoparticles as reducing and capping agents (Kumar et al., 2019). The role of this capping agent is to control the growth, aggregation, and physical and chemical properties of nanoparticles (Sidhu et al., 2022). In addition, secondary metabolites in plant extracts also play a role in stabilization, shape and size of nanoparticles (Kumar et al., 2019).

3.2. CaO nanoparticles

CaO was synthesized from $CaCl_2$ solution derived from eggshell powder which was reacted with HCl according to the reaction:

$$CaCO_3\ (s) + 2HCl\ (aq) \rightarrow CaCl_2\ (aq) + H_2CO_3(aq)$$

The color of the eggshell powder obtained is light brown. Eggshell powder containing $CaCO_3$ can react with HCl to produce a $CaCl_2$ solution. In this reaction process H_2CO_3 is also formed which is characterized by CO_2 gas bubbles that appear during stirring. The $CaCl_2$ solution acts as a source of Ca which is used in the synthesis of CaO nanoparticles. Calcium oxide synthesized in this study included: CaO-0 from $CaCl_2$ solution by calcination method and CaO-1 synthesized from $CaCl_2$ solution by adding *Cymbopogon citratus* extract in a ratio of 50:50 CaO powder the resulting white.

3.3. UV-Vis spectra of CaO nanoparticles

The extracts of *C. citratus*, CaO-0 and CaO-1 were characterized using a UV-Visible spectrophotometer to determine the wavelength shift and the maximum wavelength. This confirms the formation of CaO nanoparticles. The UV-Vis spectra of CaO are shown in **Figure 1**. The synthesis was carried out by adding water extract of lemongrass leaves (CC extract) with $CaCl_2$ solution from eggshells. The formation of CaO particles is seen with the characteristics of the mixed color from green to white.

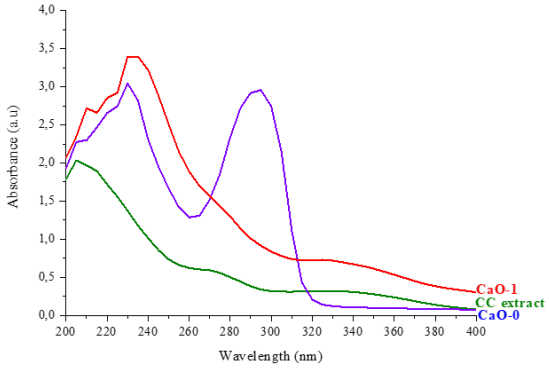

Figure 1. UV-Vis spectra of CaO nanoparticles.

The *C. citratus* extract has a maximum wavelength in the ultraviolet (UV) region. This maximum wavelength shifted when *C. citratus* extract was used to synthesize CaO nanoparticles. The more the amount of $CaCl_2$ solution used in the synthesis of CaO nanoparticles, the maximum wavelength shifts to the right and the absorbance is higher. The maximum wavelength with the highest absorbance is indicated by CaO-1. The process of biosynthesis of CaO particles using lemongrass leaf water extract is formed due to the reaction that occurs between polyphenol compounds and Ca^{2+}. This characterization is

related to the analysis of surface plasmon resonance (SPR) that occurs in colloidal CaO particles. The maximum wavelength with the highest absorbance was shown by CaO-1 at 230 nm and 330 nm. Calcium oxide which was synthesized without using *C. citratus* extract (CaO-0) had two maximum wavelengths in the UV and visible regions, namely 230 nm and 295 nm. This is in accordance with previous research, the synthesis of CaO with broccoli extract which resulted in the absorption of UV-vis waves in the range of 297 nm (Osuntokun et al., 2018). From the shift in wavelength value, it can be concluded that the resulting CaO nanoparticles have been formed.

Infrared spectroscopy is a technique based on molecular vibrations or transitions in the vibrational and rotational levels of molecules. This spectroscopy provides information about the different functional groups that appear on the surface of the nanoparticles (Ramola & Joshi, 2019). Calcium oxide was analyzed using FT-IR to determine the functional groups and Ca-O bonds that occur. The FT-IR spectra of CaO-0 and CaO-1 are shown in **Figure 2.** The spectrum clearly shows the formation of CaO.

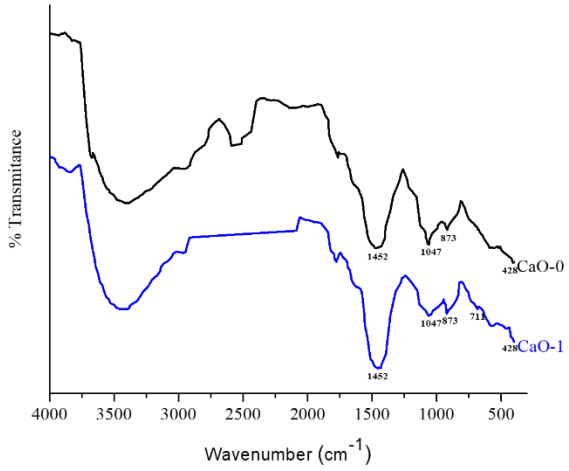

Figure 2. FT-IR spectra of CaO nanoparticles

Based on the resulting FT-IR spectra, a wide absorption band is formed at a wave number of 3400 cm^{-1}, indicating O-H bonds of water molecules on the CaO surface (Maringgal et al., 2020). The absorption bands that appear in the wave number region of 1452, 1047, and 873 cm-1 indicate the presence of C−O bonds which indicate that carbonation occurs in CaO nanoparticles (Habte et al., 2019). At a wave number of 428 cm-1, it shows the Ca−O vibrational band. In addition, the small absorption band that appears at the wavenumber 711 cm^{-1} also indicates the presence of Ca−O bonds that identify CaO (Bano & Pillai, 2020). The C=O bond is indicated by the absorption band at wave number 1795 cm^{-1}(Ramola & Joshi, 2019).

3.4. XRD diffractogram of CaO nanoparticles

XRD testing of the sample was carried out to identify the composition and phase of the sample. Structural characterization and identification of the CaO phase were carried out on CaO-0 and CaO-1. X-ray diffraction (XRD) is a non-destructive analysis which is very important for the characterization of materials. The XRD technique is based on X-ray diffraction on powders or crystalline materials and the resulting diffractogram represents the intensity at two theta (2θ) angle scattering. Structural characterization and identification of the CaO phase were carried out on CaO-0 and CaO-1. The XRD diffractogram is shown in **Figure 3**. The resulting diffractogram pattern still contains an amorphous phase, this indicates that the CaO obtained from the synthesis is not pure CaO. The main peak of CaO-0 appears at 2θ° = 18.0°; 29.4°; and 34.1° and another high-intensity peak appears at 2θ° = 31.8°; 39.4°; 43.1°; 47.1°; 50.8°; 54.3°; 62.8°; and 71.8°. The main peak of CaO-1 appears at 2θ° = 17.9°; 29.4°; 31.7°; and 34° and another high-intensity peak appears at 2θ° = 25.8°; 28.3°; 32.8°; 39.3°; 46.9°; 50.7°; 54.3°; 62.5°; and 71.4°. The XRD diffractograms of CaO-0 and CaO-1 exhibit similar patterns, however, slight differences in intensity are observed, and certain peaks appear in CaO-1 that are absent in CaO-0. The diffractogram peaks of $CaCO_3$, $Ca(OH)_2$ and CaO are seen in these two samples (Gurav et al., 2020; Nuryantini et al., 2019). This confirms that the resulting CaO is not pure CaO. The particle size of the

calcium oxide nanoparticles was calculated using the Scherrer formula:

$$D = \frac{k\lambda}{\beta \cos\theta}$$

Where D is a measure of crystallinity (Å), which is an X-ray wavelength (Å), is a full width at half maximum / FWHM (rad), is a Bragg diffraction angle and k is a constant (0.94). The particle size of crystalline CaO-0 based on calculations using the Debye Scherrer formula ranged from 33.72 - 38.48 nm while the particle size of crystalline CaO-1 ranged from 28.93 - 70.75 nm.

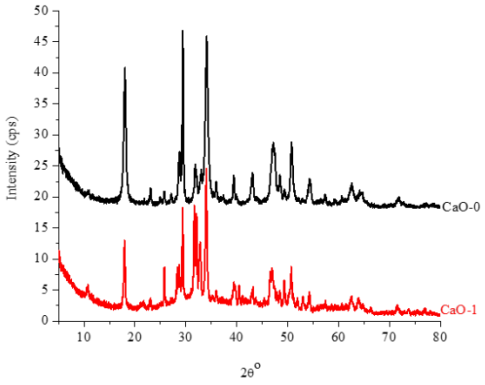

Figure 3. CaO nanoparticle diffractogram

The results of the characterization using XRD were analyzed using the *Match!* as shown in **Figure 4** and **Figure 5**. The figure shows the types of calcium oxide phases in CaO-0 identified, namely 48.7% calcite, 37.3% aragonite, and 14% calcium carbonate calcite. Identified calcite has a trigonal crystal system, aragonite has a triclinic crystal system, while calcium carbonate calcite has a rhombohedral crystal system.

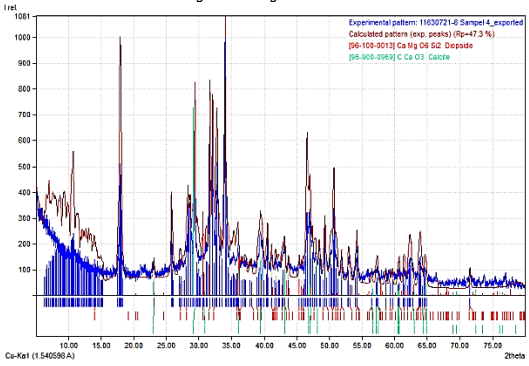

Figure 4. *Match!* result of CaO-0

Based on the results in **Figure 4** and **Figure 5**, the phases identified in the CaO-1 diffractogram are 56.8% diopside and 43.2% calcite. The crystal system in diopside is monoclinic while in calcite it is trigonal.

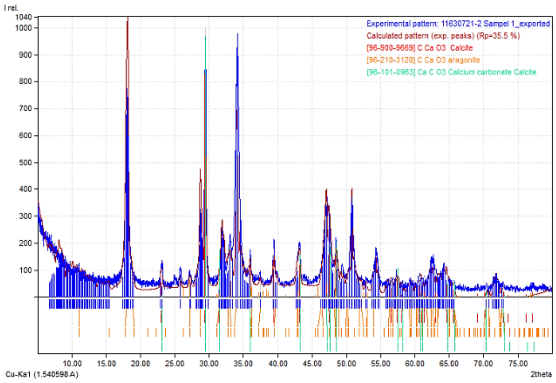

Figure 5. *Match!* result CaO-1

3.5. CaO surface morphology

The surface morphology of CaO-0 and CaO-1 were characterized using SEM-EDX. The resulting SEM micrograph is shown in **Figure 6**. Based on this figure, the shape of CaO-0 particles is more regular than CaO-1. The surface of CaO-0 appears as an irregular cube, while CaO-1 forms irregular spherical lumps, as observed in the SEM micrographs. This is consistent with the results of the XRD diffractogram which shows that CaO-0 has more ordered particles than CaO-1 and is more crystalline. Calcium oxide in CaO-1 obtained is not pure.

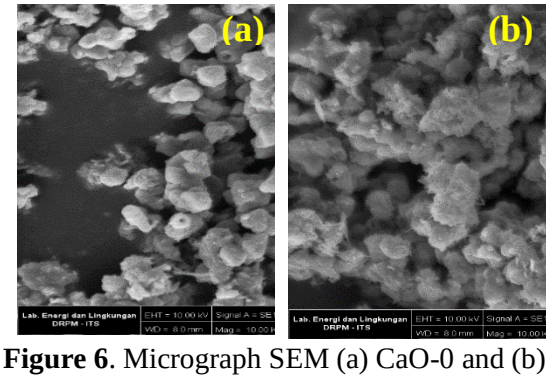

Figure 6. Micrograph SEM (a) CaO-0 and (b) CaO-1

Energy Dispersive X-Ray generally involves an X-ray spectrum for scanning the SEM region. The results obtained represent

the elemental composition in CaO-0 and CaO-1 in the form of Ca and O (**Figure 7**). The percentage of Ca in CaO-0 is higher than in CaO-1, with values of 19.8% and 14.7%, respectively (**Table 2**). The lower Ca content in CaO-1 may be attributed to the interaction between calcium precursors and the bioactive compounds present in *C. citratus* extract. The presence of phytochemicals such as flavonoids, tannins, and triterpenoids could influence the reduction and stabilization of CaO nanoparticles, potentially leading to the formation of additional organic residues or secondary phases. Moreover, the XRD results indicate that CaO-1 contains a diposide phase, which suggests that the synthesis using *C. citratus* extract may have facilitated the incorporation of other elements, thereby reducing the overall Ca percentage compared to CaO-0.

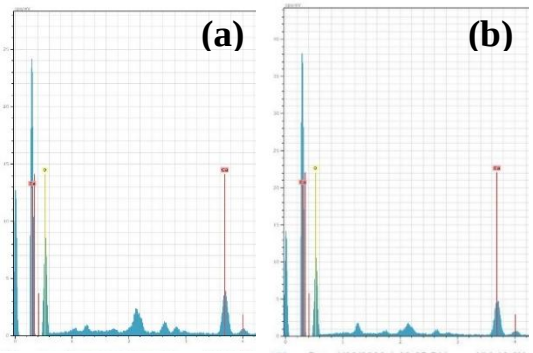

Figure 7. EDX spectra of (a) CaO-0 and (b) CaO-1

Table 2. Elemental composition of CaO

No.	Element	Composition (%)	
		CaO-0	CaO-1
1	Ca	19,8	14,7
2	O	80,2	85,3

4. CONCLUSIONS

The results showed that *C. citratus* can be used in the synthesis of CaO nanoparticles because it contains alkaloids, flavonoids, triterpenoids, and tannins. These compounds act as reducing and capping agents. Comparison of the composition of eggshell powder with the optimum *C. citratus* extract at 50:50 v/v. Characterization using a UV-Vis spectrophotometer showed that the maximum absorption of CaO nanoparticles occurred at wavelengths of 230 and 330 nm. The presence of *C. citratus* extract played a crucial role in shifting the absorption bands, indicating its involvement in nanoparticle stabilization and formation. Compared to CaO synthesized without the extract, the UV-Vis spectra of CaO-1 (50:50 composition) exhibited a more defined peak, suggesting enhanced nanoparticle dispersion and reduced aggregation. CaO-0 and CaO-1 have amorphous and crystalline structures containing a calcite phase with a crystal size of CaO-0 particles ranging from 33.72 - 38.48 nm while the crystal size of CaO-1 particles ranging from 28.93 - 70.75 nm. SEM-EDX results that the elemental composition on the surface of calcium oxide in the form of Ca and O is not homogeneous. CaO-0 is shaped like an irregular cube while CaO-1 forms rough spherical lumps.

ACKNOWLEDGMENT

The author would like to thank the Institute for Research and Community Service (LPPM) of the University of Nusa Bangsa (UNB) Bogor which has provided material support for the research and writing of this scientific paper.

LIST OF REFERENCES

Ain Samat, N., & Md Nor, R. (2013). Sol-gel synthesis of zinc oxide nanoparticles using Citrus aurantifolia extracts. *Ceramics International*, *39* (SUPPL.1), 1–4. https://doi.org/10.1016/j.ceramint.2012.10.132

Anantharaman, A., & George, M. (2016). Green Synthesis of Calcium Oxide Nanoparticles and Its Applications. *Journal of Engineering Research and Application Www.Ijera.Com*, *6*(10), 27–31.

AOAC. (1990). *Official Methods of analysis 15th edn, Association of official analytical Chemist*.

Balakrishnan, B., Paramasivam, S., & Arulkumar, A. (2014). Evaluation of the lemongrass plant (Cymbopogon citratus) extracted in different solvents for antioxidant and antibacterial activity against human pathogens. *Asian Pacific Journal of Tropical Disease*, *4*(S1). https://doi.org/10.1016/S2222-1808(14)60428-X

Bano, S., & Pillai, S. (2020). Green synthesis of calcium oxide nanoparticles at different calcination temperatures. *World Journal of Science, Technology and Sustainable Development*, *17*(3), 283–295. https://doi.org/10.1108/wjstsd-12-2019-0087

Ćujić, N., Šavikin, K., Janković, T., Pljevljakušić, D., Zdunić, G., & Ibrić, S. (2016). Optimization of polyphenols extraction from dried chokeberry using maceration as traditional technique. *Food Chemistry*, *194*, 135–142. https://doi.org/10.1016/j.foodchem.2015.08.008

Fatimah, I., Hidayat, H., Nugroho, B. H., & Husein, S. (2020). Ultrasound-assisted biosynthesis of silver and gold nanoparticles using Clitoria ternatea flower. *South African Journal of Chemical Engineering*, *34*(June), 97–106. https://doi.org/10.1016/j.sajce.2020.06.007

Gagan Shah, Richa Shri, Vivek Panchal, Narender Sharma, Bharpur Singh, A.S.Man. (2011). Scientifi c basis for the therapeutic use of Cymbopogon citratus, Stapf (Lemon grass). *Journal of Advanced Pharmaceutical Technology & Research*, *2*(1), 3.

Goli, J., & Sahu, O. (2018). Development of heterogeneous alkali catalyst from waste chicken eggshell for biodiesel production. *Renewable Energy*, *128*, 142–154. https://doi.org/10.1016/j.renene.2018.05.048

Gurav, V. L., Samant, R. A., Manjare, S. B., Patil, U. K., Solkar, S. R., & Moghe, S. S. (2020). Asian Journal of Nanoscience and Materials Biosynthesis of calcium oxide nanoparticles using Ocimum sanctum (Tulsi) leaf extracts and screening its antimicrobial activity. *Asian Journal of Nanoscience and Materials*, *3*, 415639.

Habte, L., Shiferaw, N., Mulatu, D., Thenepalli, T., Chilakala, R., & Ahn, J. W. (2019). Synthesis of nano-calcium oxide fromwaste eggshell by sol-gel method. *Sustainability (Switzerland)*, *11*(11), 1–10. https://doi.org/10.3390/su11113196

Iravani, S. (2011). Green synthesis of metal nanoparticles using plants. *Green Chemistry*, *13*(10), 2638–2650. https://doi.org/10.1039/c1gc15386b

Kumar, I., Mondal, M., & Sakthivel, N. (2019). Green synthesis of phytogenic nanoparticles. In *Green Synthesis, Characterization and Applications of Nanoparticles*. Elsevier Inc. https://doi.org/10.1016/b978-0-08-102579-6.00003-4

Laca, A., Laca, A., & Díaz, M. (2017). Eggshell waste as catalyst: A review. *Journal of Environmental Management*, *197*, 351–359. https://doi.org/10.1016/j.jenvman.2017.03.088

M. Umar, I. Mohammed, J. Oko, I. Tafinta, A. Aliko, and D. Jobbi. (n.d.). Hytochemical Analysis and Antimicrobial Effect of Lemon Grass (Cymbopogon citratus) Obtained From Zaria, Kaduna State, Nigeria. *J. Complement. Altern. Med. Res*, *1*(2), 1–8. https://doi.org/doi: 10.9734/jocamr/2016/26783

Maringgal, B., Hashim, N., Tawakkal, I. S. M. A., Hamzah, M. H., & Mohamed, M. T. M. (2020). Biosynthesis of CaO nanoparticles using Trigona sp. Honey: Physicochemical characterization,

antifungal activity, and cytotoxicity properties. *Journal of Materials Research and Technology*, *9*(5), 11756–11768. https://doi.org/10.1016/j.jmrt.2020.08.054

Marquis, G., Ramasamy, B., Banwarilal, S., & Munusamy, A. P. (2016). Evaluation of antibacterial activity of plant mediated CaO nanoparticles using Cissus quadrangularis extract. *Journal of Photochemistry and Photobiology B: Biology*, *155*, 28–33. https://doi.org/10.1016/j.jphotobiol.2015.12.013

Nuryantini, A. Y., Sundari, C. D. D., Halimahtussa'diah, H., & Nuryadin, B. W. (2019). Synthesis and Characterization of Calcium Oxide Nanoparticles from Duck Eggshells using Ball Milling Methods. *Jurnal Kimia Valensi*, *5*(2), 231–135. https://doi.org/10.15408/jkv.v5i2.8779

Osuntokun, J., Onwudiwe, D. C., & Ebenso, E. E. (2018). Aqueous extract of broccoli mediated synthesis of CaO nanoparticles and its application in the photocatalytic degradation of bromocrescol green. *IET Nanobiotechnology*, *12*(7), 888–894. https://doi.org/10.1049/iet-nbt.2017.0277

Poinern, G. E. J., & Fawcett, D. (2019). Sustainable utilization of renewable plant-based food wastes for the green synthesis of metal nanoparticles. In *Harnessing Nanoscale Surface Interactions: Contemporary Synthesis, Applications and Theory*. Elsevier Inc. https://doi.org/10.1016/B978-0-12-813892-2.00001-X

Ramola, B., & Joshi, N. C. (2019). Green Synthesis, Characterisations and Antimicrobial Activities of CaO Nanoparticles. *Oriental Journal of Chemistry*, *35*(3), 1154–1157. https://doi.org/10.13005/ojc/350333

Sidhu, A. K., Verma, N., & Kaushal, P. (2022). Role of Biogenic Capping Agents in the Synthesis of Metallic Nanoparticles and Evaluation of Their Therapeutic Potential. *Frontiers in Nanotechnology*, *3*, 801620. https://doi.org/10.3389/fnano.2021.801620

Smitha, P. S., Sheeja, T. T., & Manju, M. (2020). Green nanoparticles from different plant groups. In *Phytonanotechnology: Challenges and Prospects*. Elsevier Inc. https://doi.org/10.1016/B978-0-12-822348-2.00004-8

Stadelman E.J. (2015). *Eggs and Egg Products* (F. F.J., Ed.; Second). John Willey.

Yoonus, J., Resmi., R., & Beena, B. (2020). Greener nanoscience: Piper betel leaf extract mediated synthesis of CaO nanoparticles and evaluation of its antibacterial and anticancer activity. *Materials Today: Proceedings*. https://doi.org/10.1016/j.matpr.2020.05.246

Jurnal Ilmiah Berkala: Sains dan Terapan Kimia
Vol. 19 No. 1, Januari 2025

Application of Palm Solid Waste Ash as A Ceramic Glazing Material

Penerapan Abu Limbah Padat Sawit sebagai Bahan Glatsir Keramik

Caecilia Tridjata Suprabanindya[1], Himawan Tri Bayu Murti Petrus[2], Fariz Al Hazmi[3*]

[1]Departemen of Visual Art Education, Universitas Negeri Jakarta, Jakarta 13220, Indonesia
[2]Departemen of Chemical Engineering, Universitas Gajah Mada, Special Region of Yogyakarta 55281, Indonesia
[3]Departemen of Visual communication design, Universitas Indraprasta PGRI, Jakarta 13220, Indonesia

Email: farizalhazmi16@gmail.com

ABSTRACT

The aim of this research is to develop a glaze from palm oil solid waste ash. Oil palm plants were chosen because the ash of palm fronds, stems and trees have not been utilized optimally, only used as organic fertilizer and material for making furniture. This research is applied research involving expertise in the field of fine arts, especially ceramic art and chemical engineering, with an inquiry-based research approach. Laboratory tests (EDX Report) were carried out so that the process of modifying the ash glaze formula could be carried out more accurately. The output of this research is the palm oil solid waste ash glaze formula/recipe and ash analysis table along with test pieces of ash glaze trial results and ceramic work prototypes. In practice, organic ash cannot be used alone but must be mixed with other ingredients so that it can potentially be processed into glaze. The glaze formula used in this research contains different mixtures of ingredients. In this research, organic ash was mixed with soil (Sukabumi and Kebumen) and ready-to-use frit glaze (F.107 and F.3T). Next, the ash glaze is burned at cone temperatures 5 and 6 (1150 ℃–1200 ℃). The test piece material used is Sukabumi clay which has been proven to be compatible with the oil palm plant ash glaze formula, resulting in a more varied, attractive, artistic and unique visual appearance of the work.
Keywords: Ceramics, Glaze Ash, Waste, Palm Oil, natural materials

ABSTRAK

Penelitian ini bertujuan untuk mengembangkan glasir dari abu limbah padat kelapa sawit. Tanaman kelapa sawit dipilih karena abu pelepah, batang dan pohon kelapa sawit belum dimanfaatkan secara optimal, hanya digunakan sebagai pupuk organik dan bahan pembuatan furnitur. Penelitian ini merupakan penelitian terapan yang melibatkan keahlian di bidang seni rupa khususnya seni keramik dan teknik kimia, dengan pendekatan penelitian berbasis inkuiri. Uji laboratorium (EDX Report) dilakukan agar proses modifikasi formula ash glasir dapat dilakukan dengan lebih akurat. Luaran penelitian ini berupa formula/resep glasir abu limbah padat kelapa sawit dan tabel analisis abu beserta potongan uji hasil uji coba abu glasir dan prototipe karya keramik. Dalam praktiknya, abu organik tidak dapat digunakan sendiri, melainkan harus dicampur dengan bahan lain sehingga berpotensi diolah menjadi glasir. Formula glasir yang digunakan dalam penelitian ini mengandung campuran bahan yang berbeda-beda. Pada penelitian ini abu organik dicampur dengan tanah (Sukabumi dan Kebumen) dan frit glasir siap pakai (F.107 dan F.3T). Selanjutnya abu glasir dibakar pada suhu kerucut 5 dan 6 (1150 ℃–1200 ℃). Bahan uji benda uji yang digunakan adalah tanah liat Sukabumi yang telah terbukti kompatibel dengan formula glasir abu tanaman kelapa sawit sehingga menghasilkan tampilan visual karya yang lebih bervariasi, menarik, artistik dan unik.

Kata Kunci : Keramik, Abu Glatsir, Limbah, Kelapa Sawit, bahan alam.

Received: 27 June 2024; **Accepted**: 30 December 2024: **Available online**: 30 January 2025

1. INTRODUCTION

Ceramic technology experimentation activities have resulted in the formulation of new ceramic base materials and glazes as well as new ceramic firing formation techniques. Ceramics are objects whose manufacturing process uses soil or silicate rock and through a high temperature firing process (Ferrer et al, 2015; Rahaman, 2017; Yustana, 2020; Dadkhah et al, 2023). In making ceramics, glazing is a common method for producing a layer of color on the body of the ceramic (Pradell, and Molera, 2020). The beauty of a glaze is influenced by several factors, including the suitability of the type and technique of the glaze to the shape of the ceramic, surface quality, texture and color of the glaze and maturity of the glaze.

Aesthetic value comes from the concept of art personally and the most important thing is the artist's way of thinking (Jamuni, 2016; Murphy, 2023). The function of using glaze is to close the pores of the ceramic body so that the ceramic is watertight and makes the ceramic stronger and more resistant to weather disturbances, chemicals and general physical disturbances such as scratches (Anufrik et al, 2016). Apart from that, the glaze layer also provides beauty and uniqueness through the unique color and texture of the glaze (Said et al, 2014; Muhdy et al, 2017; Kalilu and MICHAEL, 2021).

Glazes on ceramic works are generally made from mineral and oxide materials that are insoluble in water with the main element being silica, which is alkaline, neutral and acidic with the molecular formula $RO_2-R_2O_3-RO_2$ and sodium soda. The glaze component is a combination of one or more basic oxides (flux), acid oxides (silica) and neutral oxides (alumina) (Sianita et al, 2017) Colorants for chemical glazes are obtained from mineral rocks which produce coloring oxides such as: iron oxide (FeO), copper oxide (CuO_2), cobalt oxide (CoO) and other rock minerals. Apart from oxide glaze, there is an ash (organic) glaze which can be used as a glaze after mixing it with other ingredients such as lime, feldspar, ball clay and silica. Some of the ash derived from plants can be used as a material for making decorative ceramics [Muhamad Nor and Hazwani, 2016; Muangkaew, 2022; Schettino and Holand, 2015). Using ash from plants produces a unique texture in ceramic work and a different character than in general (Putra and Deni, 2019). The results of burning ash glaze are no less interesting than glaze in general. The unique, natural feel of the texture and color of the ash glaze is its own attraction. Adding ash to ceramic glaze is rarely done by craftsmen and ceramicists in Indonesia. They seem more interested in using factory-made glaze formulas that are ready to use and practical to process, but the price is relatively expensive because the glaze coloring ingredients must be exported from abroad.

One sector that is Indonesia's mainstay or advantage is plantations, especially the commodity palm oil. Researchers are interested in choosing palm oil waste which is the remains from the process of cultivating oil palm plants and from the palm oil processing industry. Palm oil waste is the remains of oil palm plants which are not included in the materials used in the production process, so they are wasted and have not been utilized (Haryanti et al, 2014; Harahap, 2017). Every

year palm oil production increases, so there will be an increase in waste from the Palm Oil Processing industry. Even though organic waste can decompose, the accumulation of organic waste also needs to be reduced so that it can be controlled and not pollute the environment (Oetopo et al, 2021; wang et al, 2023). Efforts to process palm oil solid waste by the government and entrepreneurs have been carried out but are not yet optimal, especially for solid waste. So far, palm oil solid waste has only been used as organic fertilizer for plants. The type of waste chosen to be used in this research is solid palm oil waste in the form of empty bunches, shells and palm fiber which are burned and turned into ash. According to several studies, natural biomaterials are commonly non-toxic, non-polluting and harmless to health, and have antioxidants and antimicrobials which add to the positive effects of these natural material (Aishwarya and Anchana, 2014; Sun et al, 2023). From the point of view of ceramic art, the use of waste can be an impetus for the development of creative media and innovation (Marwanto et al, 2022).

It is hoped that mixing the basic glaze ingredients and ash extract from palm oil solid waste will produce an attractive natural color effect because the color and texture of the resulting glaze are never the same. This difference in visual characteristics is caused by the fact that the mineral content in the clay where oil palm grows is not the same. All these natural transformation processes occur in a burning furnace which involves the three main natural elements, namely: air, earth and water. Apart from that, the ash glaze processing technique and the glazing technique also have a big influence on the texture and surface properties of the glaze.

2. MATERIALS AND METHODS

2.1. Materials

The material in this research is palm oil waste ash from combustion taken from two places. The first waste is taken from PT. Pugung Raya is in Banyu Irang Village, Bati Bati, South Kalimantan and the second waste is taken from PT. Austindo Nusantara Jaya Agri, Binanga, North Sumatra. Then, the ceramic material is clay taken from Sukabumi and Kebumen as well as glazing material.

2.2. Methods

This research is interdisciplinary research involving expertise in the field of fine arts, especially ceramic art and chemical engineering. The research method uses an experimental method with a one-shot case study type pre-experimental approach. The experimental research method is a method used to find the effect of certain treatments on others under controlled conditions (Sugiyono, 2015). The analysis process for the application uses descriptive qualitative by looking at the results of the application of palm ash waste to ceramic products. The stages in this research are as follows:

a. Element content of Palm Oil Solid Waste Ash using EDX. This step is carried out so that the process of modifying the ash glaze formula can be carried out more accurately.
b. Element content in soil used as raw material for making ceramics using EDX. Soil content tests are carried out to determine soil content that can affect results.
c. Making Test Pieces and Prototypes of Ceramic Works which are carried out to apply the results of the formulas made into ceramic works and analyzing the prototype results.

3. RESULTS AND DISCUSSION

3.1. Laboratory Test of Element Content in Palm Oil Solid Waste Ash and Clay

The first stage carried out was carrying out an EDX test on two types of palm ash. This was done to determine and analyze the mineral element content in palm oil solid waste ash originating from Sumatra and Kalimantan Islands. The results showed that there were a difference in chemical elements for each type of ash (Figure 1, Figure 2, Figure 3, and Figure 4). The lab test process was also carried out on the Frit Glaze and the type of clay that will be used in this ash glaze research. The results of the elemental analysis of the 2 variants of Palm Oil solid waste ash showed that the elemental composition of each sample was as shown in the following data.

Figure 1 showed that the results of chemical lab tests on Palm Oil Solid Waste Ash contained 9 mineral elements which had a percentage of more than 1 %, namely: K 11.455 %, Ca 26.324 %, Si 36.235 %, S 1.113 %, Fe.17.973 %. Al 2.586 %, P. 1.174 %, Ti 1.145%, Mn. 1,127 %. The table shows that Kalimantan palm oil ash is rich in iron oxide (Fe_2O_3) content of 17,973 %. If a glaze is made, the presence of iron oxide is used as a dye and melter, strengthener and thickener for the resulting glaze (Hartono, 1983). The color of the glaze produced with iron oxide ranges from brown, ocher yellow and greenish. Apart from that, there is also a manganese oxide (MnO) content of 1.127 % which has the potential to be used as a coloring in glazes even though the content is relatively small. The glaze color produced by the element Manganese (Mn), which has metal characteristics similar to iron oxide (Fe), will produce brown and purplish colors. Meanwhile, the Ti content of 1.145 % gives the glaze a pale gray color effect.

As shown in Figure 2, the chemical lab test results (EDX Report) on Palm Oil Solid Waste Ash, there are 5 mineral elements that have a percentage of more than 1 %, namely: K 71.493 %, Ca 17.050 %, Si 6.720 %, S 1.233 % and P 1.227 %. These five minerals will affect the quality of the palm oil solid waste ash glaze produced. There is a very large potassium element of 71.49 % which has the potential to be used as a coloring in glaze. The color produced by the mineral Potassium Carbonate (K_2CO_3) is a shiny opaque white that resembles pearl white. The mineral element Si or Silicon 6,720 % in Sumatran palm oil solid waste has the potential to form a strong framework and tend to have a slightly glossy effect when used as a glaze mixture. After the lab test process on palm oil waste, the next process is to carry out lab tests on the clay used.

As shown in Figure 3, the chemical lab test results (EDX Report) on Sukabumi Clay, there are 6 mineral elements that have a percentage of more than 1 %, namely: K 15.502 %, Ca 1.012 %, Si 55.718 %, Fe 5.485 %, Al 16.703%, Ti 3.829 %. The mineral element Potassium 15.502 % in Sukabumi clay has the potential to form a thick white glaze or opaq and tends to be dull if used as a glaze mixture. This type of glaze is known as Clay Glaze which is a development from Engobe to Glaze on the surface of the ceramic body. Engobe is a ceramic coloring technique with a composition containing more natural ingredients and is commonly used in traditional ceramic making (Yana et al, 2013). The relatively large Si content of 55.718 % will strengthen the ceramic body frame and give a slightly thick effect to the glaze. Furthermore, the mineral Fe 5.485 % has the potential to produce yellow ocher and yellowish-brown colors if used as a coloring in glaze. The percentage of coloring oxide determines the quality of the color produced.

EDX Report Report No.

Sample Information

Sample Name	Limbah sawit kalimantan
Meas. Date	2022/11/15 11:36:59
Comment	Comment
Group	Elemental Analysis
Operator	Wisnu S

Measurement Condition

Channel	kV	uA	Filter	Acq.	Collimator Analysis	10mm Time	Atmos. DT%	Air
Al-U	50	45-Auto	----	0 - 40	0.00-40.00	Live- 100	30	
C-Sc	15	510-Auto	----	0 - 20	0.00- 4.40	Live- 100	30	

Quantitative Result

Analyte	Result		Std.Dev.	Calc.Proc	Line	Intensity
Si	35.235	%	[0.355]	Quan-FP	SiKa	1.7159
Ca	26.324	%	[0.096]	Quan-FP	CaKa	12.6316
Fe	17.973	%	[0.065]	Quan-FP	FeKa	149.5154
K	11.455	%	[0.067]	Quan-FP	K Ka	4.4997
Al	2.586	%	[0.348]	Quan-FP	AlKa	0.0363
P	1.174	%	[0.135]	Quan-FP	P Ka	0.0838
Ti	1.145	%	[0.046]	Quan-FP	TiKa	2.6158
Mn	1.127	%	[0.015]	Quan-FP	MnKa	6.9058
S	1.113	%	[0.058]	Quan-FP	S Ka	0.2076
Cu	0.580	%	[0.018]	Quan-FP	CuKa	6.4576
Sr	0.325	%	[0.009]	Quan-FP	SrKa	9.7245
Rb	0.323	%	[0.010]	Quan-FP	RbKa	8.9028
Zn	0.259	%	[0.014]	Quan-FP	ZnKa	3.4132
Ag	0.181	%	[0.027]	Quan-FP	AgKa	1.4865
Cr	0.092	%	[0.019]	Quan-FP	CrKa	0.4400
V	0.071	%	[0.024]	Quan-FP	V Ka	0.2397
Os	0.038	%	[0.035]	Quan-FP	OsLa	0.1925

Figure 1. Elemental Composition of Kalimantan Palm Oil Solid Waste Ash

EDX Report Report No.

Sample Information

Sample Name	Limbah sawit sumatera
Meas. Date	2022/11/15 11:42:33
Comment	Comment
Group	Elemental Analysis
Operator	Wisnu S

Measurement Condition

Channel	kV	uA	Filter	Acq.	Collimator Analysis	10mm Time	Atmos. DT%	Air
Al-U	50	58-Auto	----	0 - 40	0.00-40.00	Live- 100	30	
C-Sc	15	381-Auto	----	0 - 20	0.00- 4.40	Live- 100	29	

Quantitative Result

Analyte	Result		Std.Dev.	Calc.Proc	Line	Intensity
K	71.493	%	[0.124]	Quan-FP	K Ka	78.8220
Ca	17.050	%	[0.063]	Quan-FP	CaKa	10.5452
Si	6.720	%	[0.091]	Quan-FP	SiKa	1.0595
S	1.233	%	[0.015]	Quan-FP	S Ka	1.0600
P	1.227	%	[0.039]	Quan-FP	P Ka	0.4157
Fe	0.776	%	[0.008]	Quan-FP	FeKa	11.8557
Rb	0.491	%	[0.003]	Quan-FP	RbKa	34.8422
Mn	0.270	%	[0.005]	Quan-FP	MnKa	2.9358
Zn	0.244	%	[0.004]	Quan-FP	ZnKa	8.1919
Sr	0.191	%	[0.003]	Quan-FP	SrKa	14.6437
Cu	0.149	%	[0.004]	Quan-FP	CuKa	4.2199
Br	0.086	%	[0.003]	Quan-FP	BrKa	5.1877
Ti	0.054	%	[0.012]	Quan-FP	TiKa	0.1948
Zr	0.018	%	[0.002]	Quan-FP	ZrKa	1.4960

Figure 2. Elemental Composition of Sumatran Palm Oil Solid Waste Ash

EDX Report Report No.

Sample Information

Sample Name	Tanah Sukabumi- dtk
Meas. Date	2018/11/14 10:20:15
Comment	Comment
Group	Elemental Analysis
Operator	w isnu

Measurement Condition

Channel	kV	uA	Filter	Acq.	Collimator Analysis	10mm Time	Atmos. DT%	Air
Al-U	50	30-Auto	----	0 - 40	0.00-40.00	Live- 100	29	
C-Sc	15	433-Auto	----	0 - 20	0.00- 4.40	Live- 100	30	

Quantitative Result

Analyte	Result		Std.Dev.	Calc.Proc	Line	Intensity
Si	55.718	%	[0.378]	Quan-FP	SiKa	4.4611
Al	16.703	%	[0.303]	Quan-FP	AlKa	0.5734
K	15.502	%	[0.073]	Quan-FP	K Ka	8.9627
Fe	5.845	%	[0.030]	Quan-FP	FeKa	110.1389
Ti	3.829	%	[0.046]	Quan-FP	TiKa	19.2185
Ca	1.012	%	[0.029]	Quan-FP	CaKa	0.7573
S	0.481	%	[0.036]	Quan-FP	S Ka	0.1246
Zr	0.223	%	[0.004]	Quan-FP	ZrKa	21.0297
Cu	0.139	%	[0.008]	Quan-FP	CuKa	4.3168
V	0.138	%	[0.020]	Quan-FP	V Ka	1.0246
Rb	0.116	%	[0.005]	Quan-FP	RbKa	9.4309
Mn	0.088	%	[0.012]	Quan-FP	MnKa	1.1932
Sr	0.076	%	[0.004]	Quan-FP	SrKa	6.6635
Cr	0.043	%	[0.012]	Quan-FP	CrKa	0.4290
Y	0.037	%	[0.004]	Quan-FP	Y Ka	3.3559
Zn	0.031	%	[0.007]	Quan-FP	ZnKa	1.1489
Nb	0.019	%	[0.003]	Quan-FP	NbKa	1.8742

Figure 3. Elemental Composition of Sukabumi Clay

Sample Information

Sample Name	Tanah Kebumen
Meas. Date	2019/07/17 09:16:10
Comment	Comment
Group	Elemental Analysis
Operator	wisnu

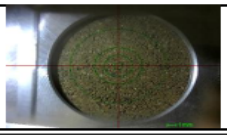

Measurement Condition

Channel	kV	uA	Filter	Acq.	Collimator Analysis	10mm Time	Atmos. DT%	Air
Al-U	50	33-Auto	----	0 - 40	0.00-40.00	Live- 100	31	
C-Sc	15	260-Auto	----	0 - 20	0.00- 4.40	Live- 100	29	

Quantitative Result

Analyte	Result		Std.Dev.	Calc.Proc	Line	Intensity
Si	38.955	%	[0.371]	Quan-FP	SiKa	3.7018
Fe	31.342	%	[0.058]	Quan-FP	FeKa	813.1933
Al	12.124	%	[0.329]	Quan-FP	AlKa	0.3919
Ca	7.034	%	[0.041]	Quan-FP	CaKa	9.5922
K	5.065	%	[0.041]	Quan-FP	K Ka	4.6906
Ti	2.371	%	[0.026]	Quan-FP	TiKa	20.2753
Tm	1.384	%	[0.006]	Quan-FP	TmLa	8.3261
Mn	0.814	%	[0.009]	Quan-FP	MnKa	16.1858
Sr	0.331	%	[0.005]	Quan-FP	SrKa	22.9777
Zr	0.125	%	[0.004]	Quan-FP	ZrKa	9.3708
Ag	0.121	%	[0.013]	Quan-FP	AgKa	2.3157
V	0.120	%	[0.011]	Quan-FP	V Ka	1.5082
Zn	0.090	%	[0.005]	Quan-FP	ZnKa	2.7936
Cr	0.049	%	[0.007]	Quan-FP	CrKa	0.8496
Ni	0.039	%	[0.006]	Quan-FP	NiKa	0.8471
Y	0.037	%	[0.003]	Quan-FP	Y Ka	2.6921

Figure 4. Elemental Composition of Kebumen Clay

The results of chemical lab tests (EDX Report) on Kebumen Clay (Figure 4) contained 7 mineral elements which had a percentage of more than 1 %, namely: K 6.065 %, Ca 7.034 %, Si 38.955 %, Fe 31.342 %, Al 12.124 %, Ti 2.371 % and Tm 1.384 %. The mineral element Si or Silicon 38.955 % in Kebumen clay has the potential to form a framework that is quite strong and tends to be somewhat glossy when used as a glaze mixture. This type of glaze is known as Earth Glaze which is a development from Engobe to Glaze on the surface of the ceramic body. The iron oxide mineral content (Fe_2O_2) which is quite large, 31.342 % in the glaze, has the potential to be a coloring agent in the glaze and as a thickener for the glaze. The resulting color can be ocher brown, dark brown or brownish green depending on the combustion temperature and the percentage of oxide content in it. The Titan oxide element (TiO2) produces a dull and opaque effect.

3.2. Process for Making Test Pieces and Prototypes of Ceramic Works

After the Laboratory Test stage, the process of making 16 test pieces is carried out in the form of small bowls with a diameter of 8 cm and a height of 6 cm. Apart from that, prototypes for ceramic works were also made in the form of 1 medium sized vase and 2 small sized vases. Making test pieces and prototypes of ceramic works is done using rotary techniques by workers at the Elina Keramik studio, Bandung. The biscuit burning process is carried out using an LPG stove at a temperature of 900 ^{0}C. Next, the glaze will be fired using cone 5 and cone 6 stakes at a temperature of 1190 ^{0}C – 1220 ^{0}C.

Furthermore, palm oil solid waste (shells) will be given the code AG.014 to indicate that Palm Oil is the 14th Organic Ash whose mineral content has been lab tested. Then the next job is to refine the leaf ash by pounding it and then filtering it twice with sizes of 60 and 80 mesh. Apart from palm oil solid waste ash, the processing process is also carried out on Sukabumi and Kebumen clay so that it is smooth enough when processed into ash glaze.

At the beginning of the glaze processing process, the solution is made slightly thicker by adding approximately 40 % water. This ash glaze is used to glaze the inside of the test piece bowl using the pouring technique. Next, to glaze the surface of the object, dip and brush techniques are used. Using these two glaze application techniques is the most suitable technique for ash glaze because it will give a unique and interesting texture effect.

The process of glazing the inside of the test piece is carried out using a pouring technique with a rather thick and thick solution mass so that the color layer and glaze surface results in better results. Then the application of ash glaze on the outside is done using a dip and brush technique. Both techniques are more suitable for ash glazes. The spray technique is not suitable because the solution mass must be finely filtered and made slightly liquid otherwise it will potentially clog the sprayer when used. Furthermore, for the decoration process of ceramic work prototypes, dip and brush techniques were used because the supply of palm ash was limited. Meanwhile, the inside is glazed using a pouring technique with frit glaze without palm ash.

The burning of all ash glaze test pieces and ceramic work prototypes was carried out using a gas furnace with a firing temperature of 1180 ^{0}C – 1220 ^{0}C for 8 hours. The ceramic objects to be fired are arranged in 3 levels. Test pieces are arranged at the bottom and middle. Meanwhile, the prototype is placed at the top. Burning is carried out in the morning from 08.00 to 16.00 in the afternoon. The new furnace opened the next day.

This ash glaze research provided results in the form of ash glaze test pieces using 4

formulas. Formulas A and B use a mixture of Frit Glaze, while formulas C and D use a mixture of Sukabumi and Kebumen clay. 4 test pieces were made for each formula so that in total there were 16 test pieces with 3 ceramic work prototypes in two sizes. Next, observations were made on 6 visual parameters which gave an overall picture of the appearance of the 014 ash glaze which was fired at a temperature of 1180 ^{0}C – 1220 ^{0}C (cone 5 and cone 6 stakes). Based on manual visual observations, the following data was obtained.

Table 1. Glaze Composition with AG.014 as Main Component

No.	Material (% b/b)	Ash Glaze Code			
		Formula A	Fomula B	Formula C	Formula D
1.	Palm Oil Solid Waste Ash (Sumatra/Kalimantan)	50	50	50	50
2.	Glaze F,107	40	-	-	-
3.	F.3T glaze	-	40	-	-
4.	Sukabumi Clay	-	-	40	-
5.	Kebumen Clay	-	-	-	40
6.	Quartz	10	10	10	10

Table 2. Observation Results of Formula A Palm Oil Solid Waste Ash Glaze

No	Visual Parameters	Test Piece Code AG.014 with Formula A			
		Formula A AG.A 014 S	**Formula A AG.A1 014**	**Formula A AG.A2 014**	**Formula A AG.A3 014**
1.	Color	pure white, plain	plain cream	ocher yellow	gray green
2.	Fluidity	Good	Good	Good	Good
3.	Shine	Semi	Matt	Matt	Semi
4.	Closing Nature	Good	Good	Good	Good
5.	Color Evenness	Good	Good	Good	Good
6.	Texture	good, soft and smooth	good, soft and smooth	good, soft and smooth	Good, a bit harsh

Overall the test piece with Formula A matured well, giving even melting and color density with matt and semi-matt glaze characteristics. The composition of ingredients in Formula A produces varied colors such as white, cream, ocher yellow and grayish green. The surface of the glaze is smooth, slippery, especially palm ash mixed with F.107 frit glaze. The fine nature of Frit glaze powder dissolves easily when mixed with palm ash. Meanwhile, the Kebumen clay mixture produces a slightly rough surface effect. To produce a smooth surface, the Kebumen clay must be ground again and

filtered finely and the glaze solution must be filtered to a size of 120 mesh. Sumatran palm ash produces a purer white with smooth and semi-matt glaze properties, while Kalimantan palm ash produces a white, slightly yellow cream effect with the same glaze properties. The cream color appears because the Fe content in Kalimantan palm ash is greater.

Table 3. Observation Results of Formula B Palm Oil Solid Waste Ash Glaze

No	Visual Parameters	Test Piece Code AG.014 with Formula B			
		Formula B AG.B 014 S	**Formula B AG.B1 014**	**Formula B AG.B2 014**	**Formula B AG.B3 014**
1.	Color	milky white, plain	white, slightly pale blue	gray on the inside, ocher yellow on the outside	milo chocolate, plain
2.	Fluidity	Good	Good	Good	Good
3.	Shine	semi	semi	semi-	Matt
4.	Closing Nature	Good	Good	Good	Good
5.	Color Evenness	Good	Good	Good	Good
6.	Texture	Good, it's a bit thick at the bottom so it's a bit lumpy	good, smooth and smooth with fine black spots	good, smooth and smooth with color gradations	Good, a bit harsh

Overall the test piece with Formula B matured well, giving even melting and color density with matt and semi-matt glaze characteristics. The composition of the ingredients in Formula B produces varied and unique colors such as pearl white, salted egg white, graded gray, ocher brown, and milo chocolate. The surface of the glaze is smooth, slippery, especially palm ash mixed with F.3T frit glaze. Meanwhile, the Kebumen clay mixture produces a slightly rough surface effect. To produce a smooth surface, the Kebumen clay must be ground again and filtered finely and the glaze solution must be filtered to a size of 120 mesh. Sumatran and Kalimantan palm ash when mixed with F.3T glaze in formula B gives a different color. Kalimantan palm ash glaze is more attractive because it has a texture of black spots.

Overall the test piece with Formula C is less mature, with visual effects like engobe. Then re-firing was carried out by adding F.107 glaze to give the glaze a glossy effect. It turned out that it was quite successful in turning engoge into a glaze, even though the surface was not smooth, it gave sufficient melting results and even color density with matt and semi-matt glaze characteristics. It is necessary to modify the composition of Formula C by adding quartz and felspard as in the composition of the 2019 ash glaze formula with a higher firing temperature. The composition of the ingredients in Formula C produces less varied colors such as dark grey, grayish brown and blackish brown. The surface of the ash glaze mixed with Sukabumi clay produces a slightly rough surface effect. To produce a smooth surface, the Sukabumi clay must be ground again and filtered finely and the glaze solution must be filtered to a size of 120 mesh.

Table 4. Observation Results of Formula C Palm Oil Solid Waste Ash Glaze

No.	Visual Parameters	Test Piece Code AG.014 with Formula C			
		Formula C AG.C 014 S	**Formula C AG.C1 014**	**Formula C AG.C2 014**	**Formula C AG.C3 014**
1.	Color	pearl white, concentrated	chocolate cream, plain	brownish grey	gray on the inside, dark brown on the outside
2.	Fluidity	not evenly distributed	Good	Good	Good
3.	Shine	Matt	semi-	semi-	Glossy
4.	Closing Nature	Enough	Good	Good	Good
5.	Color Evenness	Good	Good	Good	Good
6.	Texture	slight crawling, fine cracks	good, plain, a bit slippery	Good, a bit smooth with dark brown to gray gradations	Good, a bit slippery and crawling like orange peel on the inside

Table 5. Observation Results of Formula D Palm Oil Solid Waste Ash Glaze

No.	Visual Parameters	Test Piece Code AG.014 with Formula D			
		Formula D AG.D 014 S	**Formula D AG.D1 014**	**Formula D AG.D2 014**	**Formula D AG.D3 014**
1.	Color	rather dark grey	dark brown grey	blackish brown	blackish brown
2.	Fluidity	Good	Good	Good	Good
3.	Shine	semi-	semi-	semi-	Glossy
4.	Closing Nature	Good	Good	Good	Good
5.	Color Evenness	Good	Good	Good	Good
6.	Texture	a bit rough like sand	rough like sand	rough like sand	a bit rough like sand

Overall the test piece with Formula D is not as mature as the Formula C results, with visual effects like engobe. Then re-firing was carried out by adding F.107 glaze to give the glaze a glossy effect. It turned out that it was quite successful in turning engoge into a glaze, even though the surface was not smooth, it gave sufficient melting results and even color density with matt and semi-matt glaze characteristics. It is necessary to modify the composition of Formula D by adding quartz and feldspar as in the composition of the 2019 ash glaze formula with a higher firing temperature. The composition of the ingredients in Formula D produces less varied and unique colors such as medium gray, dark gray, grayish brown, and blackish brown. Tends to be somewhat similar. The surface of ash glaze mixed with Kebumen clay produces a slightly rough surface effect. To produce a smooth surface, the Sukabumi clay must be

ground again and filtered finely and the glaze solution must be filtered to a size of 120 mesh.

The appearance of the glaze seen on the test piece is greatly influenced by the composition of the formula as seen in formulas A, B, C and D which have special characteristics. This is where the attraction of ash glaze lies, especially since the main ingredient in palm oil solid waste ash in each location has a different mineral composition in the clay.

Figure 5. AG Test Piece Results AG.014 with Formula A, B, C, D

Figure 5 shows Test Piece AG.014 with Formulas A and B are more varied, unique and interesting than Formulas C and D. The character of the palm oil solid waste ash glaze turns out to be more successful with the composition of formulas A and B. Meanwhile, the composition of formulas C and D It must be modified again so that the nature of the Engobe changes to a more semi-glossy or glossy ash glaze with the addition of feldspar and lime and quartz elements.

3.3. Analysis of Prototype Ceramic Works

In this research, trials were also carried out on the application of ash glaze to ceramic work prototypes in the form of vases with varying sizes. The following is a visual display of the prototype:

3.3.1 Vase Work 1: Natural Antique Vase

Vase 1 has a base diameter of 9 cm and a height of 16 cm (Figure 6). The material used is Sukabumi soil which is classified as a fine earthenware type with a burning temperature of up to 1250 ^{0}C. The surface of ceramic objects is partly flat and partly textured with repeated concave lines circling the ceramic body. The glaze used is ash glaze with code AG.D 014 for the body of the vase and code AG.B1 014 for the neck of the vase. Then the entire surface is covered with F.107 glaze.

Figure 6. Natural Antique Vase Red, prototype 1 with AG 014

The brush technique was used to glaze this vase because of the limitations of the main ingredient in palm ash glaze. The glaze coating process is carried out 3 to 4 times until sufficient thickness is achieved. Next, the ceramic object is baked for 8 hours. The glaze results obtained are not all evenly colored, visible traces of circular and irregular brush strokes on the neck. Vase looks more expressive and artistic. The greenish and brownish gray color appears due to the mixture of Chrom and Fe oxides with palm ash and F.3T glaze. Meanwhile, the glaze on the body looks dull or somewhat dull with a reddish brown color. The red iron oxide mineral element in Kebumen soil contained in the composition of formula D influences the appearance of a reddish brown color. The appearance of the glaze is not too glossy so the overall appearance of Vase 1 resembles Japanese ceramic work which looks classic and unique.

3.3.2 Vase Work 2: Red Brown Engobe Vase

Figure 7. Red Brown Engobe Vase, prototype 2 with AG 014

Vase 2 has a base diameter of 14 cm and a height of 18 cm. The material used is Sukabumi soil which is classified as a fine earthenware type with a burning temperature of up to 1250 ^{0}C. The surface of ceramic objects is partly flat and partly textured with repeated concave lines circling the ceramic body. The glaze used is ash glaze with code AG.D 014 for the body of the vase and code AG.B1 014. This ash glaze uses a mixture of Sukabumi clay and Kebumen soil so that the visual appearance of the vase is stronger, characteristic of Clay Glaze which is a development of Engobe .

The brush technique was used to glaze this vase because of the limitations of the main ingredient in palm ash glaze. The glaze coating process is carried out 3 to 4 times until sufficient thickness is achieved. Next, the ceramic object is baked for 8 hours. The glaze results obtained are not shiny and tend to be dull like the character of Engobe. Circular brush marks are visible on the top of the vase. The vase appears with a brownish red engobe with a simple pattern. The brownish red color appears due to a mixture of red iron oxide and black iron oxide found in palm ash (formula C and D) and Kebumen clay and Sukabumi clay. The appearance of the glaze is not too glossy, it is quite thick with a rough surface so that the overall appearance of the Vase 2 work is quite successful in representing a unique Clay Glaze.

4. CONCLUSIONS

Based on research results, it has been confirmed that palm oil solid waste ash from Sumatra and Kalimantan can be used as raw material for ash glaze with the code AG.014. The four types of ash glaze which are formulated as Formulas A, B. C and D begin to mature at a temperature of 1150 ^{0}C – 1200 ^{0}C and the four ash glazes are coded AG.A.014, AG.B.014, AG. C. 014, AG.D. 014 produces different colors depending on the formula. The color of the 014 ash glaze is very varied, such as white, cream, blue, white and salted egg blue, ocher yellow, ocher green, milo brown, slightly dark brown, gray brown, shades of gray, indicating that the dominant coloring is iron oxide or Fe, Manganese and Chroom oxides.

The amount of fusing content in the ash glaze affects the appearance (gloss) of the ash glaze. The greater the amount of palm oil solid waste ash in the glaze, the better and more even the covering or opac properties. Ash glaze with a mixture of frit glaze formula (F.107 and F.3T) produces a clear, smooth, evenly opaque ash glaze that is beautiful and unique. Ash Glaze with a mixture of Sukabumi and Kebumen clay produces an ash glaze called Clay Glaze which looks like Engobe. Different oil palm farming locations (Sumatra and Kalimantan) affect the ash glaze produced because the mineral composition of agricultural clay in different locations has a different composition. This is the natural attraction and charm of Ash Glaze. To produce

a unique texture effect, palm oil solid waste ash is not washed first but is directly mixed with other glaze ingredients after being filtered using an 80 mesh sieve.

LIST OF REFERENCES

Aishwarya and Anchana Devi. (2014). Extraction of Natural Dyes from Fungus – An Alternate for Textile Dyeing. *Journal of Natural Sciences Research*, Vol.4, No.7.

Anufrik, S. S., Kurian, N. N., Zhukova, I. I., Znosko, K. F., and Belkov, M. V. (2016). Chemical composition of ceramic tile glazes. *Journal of Applied Spectroscopy*, 83, 764-770. https://doi.org/10.1007/s10812-016-0360-8

Dadkhah, M., Tulliani, J. M., Saboori, A., & Iuliano, L. (2023). Additive manufacturing of ceramics: Advances, challenges, and outlook. *Journal of the European Ceramic Society*. https://doi.org/10.1016/j.jeurceramsoc.2023.07.033

Ferrer, S., Mezquita, A., Gomez-Tena, M. P., Machí, C., and Monfort, E. (2015). Estimation of the heat of reaction in traditional ceramic compositions. *Applied Clay Science*, 108, 28-39. https://doi.org/10.1016/j.clay.2015.02.019

Harahap, S. (2017). Analisis Potensi Dan Strategi Pemanfaatan Limbah Kelapa Sawit di Kabupaten Labhanbatu (Doctoral dissertation, Universitas Medan Area).

Haryanti, A., Norsamsi, N., Sholiha, P. S. F., and Putri, N. P. (2014). Studi pemanfaatan limbah padat kelapa sawit. *Konversi*, 3(2), 20-29. http://dx.doi.org/10.20527/k.v3i2.161

Jamuni, P. (2016). Western Aesthetics. Bangkok: Plan Printing.

Kalilu, R. O. R., and MICHAEL, A. (2021). Cullet to glaze: Converting waste for ceramic artistic, economic and environmental development. *European Journal of Engineering and Applied Sciences*, 4(1), 1-7. https://doi.org/10.55581/ejeas.813848

Marwanto, A. B., Wahyudi, J. I., and Prasetyo, R. E. B. (2022). The creation of "repurposing" ceramic using roof tiles waste. ARTISTIC: *International Journal of Creation and Innovation*, 3(2), 160-176. https://doi.org/10.33153/artistic.v3i2.4528

Muangkaew, T. (2022). Ash glaze from durian waste for ceramic creations. *Humanities, Arts and Social Sciences Studies (Former Name Silpakorn University Journal Of Social Sciences, Humanities, And Arts)*, 755-767. https://doi.org/10.14456/hasss.2022.64

Muhamad Nor, M. A. A., and Hazwani Ya'acob, N. H. (2016). Development of Decorative Ceramic Glaze from Palm Fiber Ash. Key Engineering Materials, 690, 259-263. https://doi.org/10.4028/www.scientific.net/KEM.690.259

Muhdy, A. A., Jalil, J., and Irfan, I. (2017). *Pemanfaatan Bahan Baku Lokal untuk di Glasir Guna Meningkatkan kualitas Gerabah (Earthenware) Menjadi Keramik Di Dusun Sandi Kecamatan*

Pattallassang Kabupaten Takalar. In Prosiding Seminar Nasional" Membangun Indonesia Melalui Hasil Riset" (pp. 169-174). Lembaga Penelitian Universitas Negeri Makassar.

Murphy, A. (2023). Form and Content: A Defense of Aesthetic Value in Science. *Philosophy of Science*, 90(3), 669-685. https://doi.org/10.1017/psa.2023.46

Oetopo, R. A. A., Suprabanindya, CT, Despriliani, R., and Hazmi, F. al.(2021). Penerapan zat pewarna alami limbah organik kulit rambutan (Nephelium Lappaceum) pada bahan katun dengan teknik Shibori (tie dyes) dan batik. *Jurnal Imajinasi*, 5(1), 1-10. https://doi.org/10.26858/i.v5i1.20322

Pradell, T., and Molera, J. (2020). Ceramic technology. How to characterise ceramic glazes. *Archaeological and Anthropological Sciences*, 12(8), 189. https://doi.org/10.1007/s12520-020-01136-9

Putra, N. S. D., and Yana, D. (2019). Pemanfaatan Abu Kayu sebagai Bahan Aditif Glasir Suhu Tinggi. Jurnal Sosioteknologi, 18(3). https://doi.org/10.5614/sostek.itbj.2019.18.3.20

Rahaman, M. N. (2017). *Ceramic processing*. CRC press.

Said, T., Ramli, H., and Sedon, M. (2014). A Simple Method for Production of Eco Green Glaze from Imperata Cylindrical Ash. *ITMAR*, 1(1), 349-357.

Sianita, M. S., Darmawan, A., and Azmiyawati, C. (2017). Uji Aktivitas Fotokatalis Genteng Berglasir Silika/TiO_2 terhadap Degradasi Larutan Indigo Carmine, Metanil Yellow dan Rhodamin. *Jurnal Kimia Sains dan Aplikasi*, 20(2), 53-57. https://doi.org/10.14710/jksa.20.2.53-57

Schettino, M. A., and Hoclaya, J. N. (2015). Processing of porcelain stoneware tile using sugarcane bagasse ash waste. *Processing and Application of Ceramics*, 9(1), 17-22. https://doi.org/10.2298/PAC1501017S

Sugiyono. (2015). *Metode Penelitian dan Pengembangan Pendekatan Kualitatif, Kuantitatif, dan RandD*. Bandung: CV Alfabeta, 2015.

Sun, Y., Tian, W., Mehmood, U., Zhang, X., & Tariq, S. (2023). How do natural resources, urbanization, and institutional quality meet with ecological footprints in the presence of income inequality and human capital in the next eleven countries. *Resources Policy*, 85, 104007. https://doi.org/10.1016/j.resourpol.2023.104007

Wang, Z., Hu, Y., Wang, S., Wu, G., & Zhan, X. (2023). A critical review on dry anaerobic digestion of organic waste: Characteristics, operational conditions, and improvement strategies. *Renewable and Sustainable Energy Reviews*, 176, 113208. https://doi.org/10.1016/j.rser.2023.113208

Yana, D., Widiawati, D., and Listiani, W. (2013). Bahan Alam Engobe Sebagai Solusi Masalah Pewarna Produk Kerajinan Keramik Hias Plered Kabupaten Purwakarta. *ATRAT: Jurnal*

Seni Rupa, 1(3). http://dx.doi.org/10.26742/atrat.v1i3.390

Yustana, P. (2020). Estetika Keramik Klasik Dan Kontemporer. *Acintya*, 12(2), 170-198. https://doi.org/10.33153/acy.v12i2.3581

JURNAL ILMIAH BERKALA SAINS DAN TERAPAN KIMIA

Jurnal Ilmiah Berkala: Sains dan Terapan Kimia
Vol. 19 No. 1, Januari 2025

The Potential of Ironwood as an Activated Carbon Adsorbent for Heavy Metal Mercury (Hg) using the Pyrolysis Method

Potensi Kayu Ulin Sebagai Adsorben Karbon Aktif Untuk Logam Berat Merkuri (Hg) Menggunakan Metode Pirolisis

Zimon Pereiz[1]*, Chuchita[1], Efriyana Oksal[1], Miranti Maya Sylvani[1], Ahmad Irawan[2], Yunus Pebriyanto[3], Ruslianur Hairiah[4], Arini Eka Jaya Prastiti[4], Caroline Berlisnora Dasilva[4], Violina Anatasya[4], Risky Prisnanda[4]

[1]Department of Chemistry, Faculty of Mathematics and Natural Sciences, Universitas Palangka Raya, Palangka Raya 73111, Indonesia
[2]Department of Pharmacy, Faculty of Mathematics and Natural Sciences, Universitas Palangka Raya, Palangka Raya 73111, Indonesia
[3]Department of Physics, Faculty of Mathematics and Natural Sciences, Universitas Palangka Raya, Palangka Raya 73111, Indonesia
[4]Department of Chemistry Education, Faculty of Education and Teacher Trainimg, Universitas Palangka Raya, Palangka Raya 73111, Indonesia

Email: zimonpereiz@mipa.upr.ac.id

ABSTRACT

This study focuses on the utilization of ironwood as an activated carbon adsorbent to remove heavy metal mercury (Hg). Mercury pollution from industrial sources poses significant risks to the environment and human health. The purpose of this study was to develop an effective method for adsorbing mercury using natural ironwood materials. Activated carbon was synthesized using pyrolysis and chemically activated, followed by adsorption tests under varying pH conditions, contact times, and acid concentrations. The optimum adsorption capacity was observed at a mercury concentration of approximately 500 ppm, with maximum efficiency at pH 1 and a contact time of 80 minutes. The results also showed that the adsorption kinetics followed a second-order model with a rate of 0.017119 g/mg.min. In conclusion, the mercury adsorption process using activated carbon from ironwood followed the Langmuir isotherm model, with an adsorption capacity of 63.036 mg/g, indicating that the adsorbent had been successfully synthesized and had an effective ability to remove mercury.

Keywords: Adsorption, Activated Carbon, Ironwood, Mercury, Pyrolysis.

Received: 18 November 2024; **Accepted**: 30 December 2024: **Available online**: 30 January 2025

1. INTRODUCTION

Heavy metals are a distinct group of elements that exhibit properties similar to other metals but are typically characterized by a high atomic weight and density exceeding 4 g/cm³. These elements include transition metals with atomic numbers ranging from 22 to 34 and 40 to 50, as well as lanthanides and actinides. Due to their specific physicochemical properties, heavy metals interact uniquely with biological systems, often exhibiting distinct biochemical responses in living organisms.

Heavy metal pollution has become more common and more reports since the mercury case in Minamata, Japan, in 1953. According

to Mursyidin, D. H. (2006), the United States Environmental Agency (EPA), thirteen heavy metals are known to have negative effects on the environment. There are some of them, such as arsenic (As), lead (Pb), mercury (Hg), and cadmium (Cd). While some heavy metals play essential roles in biological functions at trace levels, others become toxic when present in excessive concentrations.

Mercury (Hg) is a heavy metal characterized by its unique physical and chemical properties, including its liquid state at room temperature, high specific gravity, and excellent electrical conductivity. These attributes make mercury a critical component in various industrial and laboratory applications. Elemental mercury exhibits a silvery-white appearance, with a freezing point of 38.87 °C, a boiling point of 356.90 °C, a specific gravity of 13.55 g/cm³, and an atomic weight of 200.6. In nature, mercury is released from volcanic emissions and seawater evaporation, contributing to its presence in the environment (Hananingtyas, 2017).

Anthropogenic activities, particularly industrial processes, are significant contributors to mercury pollution. The chlor-alkali industry, gold mining, electrical equipment manufacturing, paint production, and the fabrication of thermometers and tensiometers all utilize mercury as a primary or auxiliary component. Additionally, mercury-containing amalgam used in dental treatments, as well as fossil fuel combustion, further exacerbate environmental mercury contamination (Sudarmaji & Prasasti, 2006). Given the persistence and toxicity of mercury, efficient removal techniques are essential to mitigate its impact on ecosystems and human health.

Adsorption using natural materials has been widely explored as a cost-effective and environmentally friendly approach for mercury removal. Various studies have demonstrated the effectiveness of agricultural waste-based adsorbents, such as rice husks and water hyacinth, in capturing mercury ions (Hg^{2+}) from aqueous solutions. When treated with NaOH and activated for adsorption, water hyacinth has been shown to remove up to 94.26% of mercury within a short duration, attributed to its highly porous surface and functional groups capable of binding heavy metals. The adsorption efficiency of these materials has been evaluated through Atomic Absorption Spectroscopy (AAS) (Miftahurrahmah et al., 2017).

In addition to adsorption, mercury remediation can also be achieved through coagulation and precipitation techniques. These methods involve the addition of chemical agents such as aluminum sulfate or iron salts, which promote the aggregation and sedimentation of mercury, facilitating its removal from wastewater (Harmono, 2020). Despite the effectiveness of these approaches, further research is required to develop sustainable and highly efficient adsorbents that can enhance mercury removal from contaminated water sources.

Ironwood (*Eusideroxylon zwageri*), commonly known as Ulin wood, is a tropical hardwood species endemic to Kalimantan. It is recognized for its exceptional durability and mechanical strength, making it a valuable resource in various construction applications, including residential structures, bridges, railroad sleepers, electric poles, and maritime vessels (Sidiyasa & Juliaty, 2003; Baroya et al., 2023). Due to its Class I durability rating, ironwood is often referred to as "Iron Wood," and its properties are considered superior compared to most other timber species.

Ironwood trees can attain heights exceeding 30 meters, with trunk diameters surpassing 90 cm. The species thrives under tropical rainforest conditions, preferring temperatures between 25–35 °C and annual precipitation ranging from 2500 to 3900 mm. It is commonly found at elevations of 100–600 meters above sea level, with a natural density of approximately 4–8 trees per hectare. The reproductive cycle of ironwood varies by region; in Palembang, flowering occurs between August and September, whereas in South Kalimantan, it occurs from October to November. The maturation period from flower to seed completion is approximately three months. Additionally, ironwood is frequently found growing in association with more than 100 other tree species, including *Palaquium hasseltii*, *Ochanostachys amentaceae*, and

Shorea spp. in Jambi (Hendalastuti & Siregar, 2007).

The geographical distribution of *Eusideroxylon zwageri* spans the tropical rainforests of Kalimantan, Sumatra, and parts of Malaysia. However, due to extensive deforestation and commercial exploitation, the population of this species has experienced a significant decline. In South Kalimantan, the estimated availability of ironwood in natural forests has been reduced to approximately 1.35 m^3/ha for poles and 6.82 m^3/ha for mature trees. Furthermore, inter-provincial trade contributes to its distribution, with supply chains extending from East Kalimantan and Tanjung (Yudi & Itta, 2014).

Beyond its structural applications, ironwood has demonstrated potential in environmental remediation, particularly in water treatment. It serves as a promising precursor for activated carbon production, a material known for its high surface area and effective adsorption properties. Activated carbon derived from ironwood has been utilized to remove natural organic matter (Bahan Organik Alami, BOA) from peat water. The activation process, which involves carbonization followed by chemical treatment, enhances the porosity and adsorption efficiency of the material. Consequently, ironwood-based activated carbon offers a dual benefit, functioning as both a high-value construction material and an effective adsorbent for wastewater treatment applications (Nafilah & Noor, 2021).

Activated carbon is a material that is widely used as an adsorbent because it has a high surface area and pores that are effective in capturing small molecules from liquids or gases. One potential source of activated carbon is ironwood (*Eusideroxylon zwageri*), a hardwood originating from Kalimantan and Sumatra. In addition to its strength and resistance to the environment, ironwood also has the potential to be processed into high-quality activated carbon (Nafilah, S., & Noor, R. 2021). Ironwood as a basic material for activated carbon offers several benefits and wide applications in various industries, including: (1.) Water Filtration: Activated carbon from ironwood can be used to filter water, especially in removing natural organic materials, such as in research on peat water. The adsorbent properties of activated carbon are able to bind hazardous compounds contained in water, resulting in water that is cleaner and safer for consumption. (2.) Liquid Waste Treatment: Liquid waste from industry often contains hazardous chemicals and organic compounds that are difficult to decompose. Ironwood activated carbon can be used in the liquid waste purification process to reduce contaminant levels, including organic materials and heavy metals, so that the waste produced is more environmentally friendly. (3.) Air Treatment: In air treatment, activated carbon can absorb volatile organic compounds (VOCs) and unpleasant odors. Ironwood processed into activated carbon with certain techniques has the potential to be used in air purifiers. (4.) Refining Used Cooking Oil: The use of activated carbon from ironwood has also been proven effective in refining used cooking oil through the adsorption process. This activated carbon is able to bind free fatty acids, reduce peroxide content, and improve the quality of the oil that has been used.

The process of making activated carbon from ironwood goes through several main stages, including: 1) Carbonization; The process of heating ironwood at high temperatures without oxygen to form carbon. 2) Activation; The further process of providing chemicals or water vapor to open the pores of the carbon formed, resulting in activated carbon with a high surface area. Activated carbon produced from ironwood has physical and chemical properties that are ideal for use in various filtration and adsorption applications (Oko, Syarifuddin, et al 2020).

Activated carbon is widely recognized as an effective adsorbent due to its high surface area and well-developed porosity, which facilitate the capture of small molecules from liquid and gaseous phases. This material plays a crucial role in various environmental applications, particularly in water purification, air filtration, and industrial waste treatment. One promising precursor for activated carbon production is ironwood (*Eusideroxylon zwageri*), a dense hardwood native to Kalimantan and Sumatra, known for its

exceptional strength and environmental resistance (Nafilah & Noor, 2021). Given its structural properties, ironwood presents a viable alternative for the synthesis of high-quality activated carbon with significant adsorption capabilities.

The utilization of ironwood-derived activated carbon extends across multiple industrial sectors. In water treatment, it has been shown to effectively remove natural organic matter, such as humic substances in peat water, thereby improving water quality for consumption. In industrial wastewater treatment, activated carbon plays a critical role in the adsorption of hazardous chemicals, organic pollutants, and heavy metals, reducing their environmental impact. Additionally, its application in air purification enables the removal of volatile organic compounds (VOCs) and odor control, while in the food industry, it is employed in refining used cooking oil by adsorbing free fatty acids and reducing peroxide content, thereby enhancing oil quality. These broad applications highlight the versatility and efficacy of ironwood-based activated carbon in addressing environmental challenges.

The production of activated carbon from ironwood involves two fundamental processes: carbonization and activation. Carbonization entails the thermal decomposition of ironwood in an oxygen-deficient environment to produce a carbon-rich residue. This step is followed by activation, which enhances porosity through chemical or physical means, such as treatment with activating agents (e.g., phosphoric acid or steam), ultimately increasing the surface area and adsorption capacity of the final product (Oko et al., 2020). The resulting activated carbon exhibits properties that make it highly effective for adsorption-based applications, including heavy metal removal.

Heavy metal contamination, particularly from elements such as lead (Pb), mercury (Hg), cadmium (Cd), and nickel (Ni), poses significant environmental and health risks. These metals, frequently found in industrial effluents, are persistent pollutants that accumulate in ecosystems and exhibit toxic effects even at low concentrations. The application of activated carbon in wastewater treatment has been extensively studied for its ability to sequester heavy metals through both physical and chemical adsorption mechanisms. Physical adsorption relies on Van der Waals interactions to trap metal ions within the porous matrix, while chemical adsorption involves the formation of coordination bonds between metal ions and oxygen-containing functional groups, such as carbonyl and hydroxyl groups, on the surface of activated carbon.

The reusability of activated carbon further enhances its practicality as an adsorbent, making it an economically and environmentally sustainable solution for industrial waste treatment. Several studies have demonstrated its effectiveness in heavy metal adsorption. For instance, activated carbon derived from coconut shells was reported to remove up to 85% of lead (Pb) ions from electroplating wastewater (Hidayat & Nasution, 2018). Similarly, sawdust-based activated carbon exhibited a mercury (Hg) removal efficiency of approximately 75% in mining effluent (Ramanda & Sukadana, 2020). These findings underscore the potential of ironwood-derived activated carbon as a highly efficient adsorbent for heavy metal remediation in wastewater treatment systems.

Given its high adsorption capacity, structural durability, and regeneration potential, ironwood-based activated carbon presents a promising solution for mitigating environmental pollution. This study aims to evaluate the adsorption performance of ironwood-derived activated carbon in the removal of mercury (Hg) from aqueous solutions, with a focus on optimizing adsorption conditions and understanding the underlying kinetic and isotherm models governing the process.

2. MATERIALS AND METHODS

2.1. Materials

Materials used in this study consisted of liquid waste from Jl. Mahir Mahar River (Palangka Raya, Central Kalimantan), ironwood, HCl p.a., NaOH p.a., H_3PO_4 p.a., $HgCl_2$. Additional laboratory consumables included glass wool, filter paper,

demineralized water, and ice cubes. The equipment used in this study included analytical balance, magnetic stirrer, pyrolysis reactor, condenser, hose, pipe, blender, stopwatch, burette or glass box, clamp and static, water pump, knife, 100 mesh sieve, pH meter, aluminum foil, and various glassware. For material characterization and adsorption analysis, the study employed X-ray Diffraction (XRD) for phase identification, Fourier Transform Infrared Spectroscopy (FTIR) to determine functional groups, and Atomic Absorption Spectrometry (AAS) for quantifying mercury concentrations in liquid waste before and after adsorption.

2.2. Ironwood preservation

Ironwood utilized in this study was sourced from wood processing waste at CV. Banggaris Sejahtera, Palangka Raya City, Central Kalimantan Province. The raw material was thoroughly washed with deionized water to remove impurities, followed by drying in a laboratory oven at 105 °C for 24 hours to eliminate residual moisture. The dried samples were subsequently ground using a high-speed blender and sieved through a 100-mesh sieve to obtain a uniform particle size suitable for further processing.

2.3. Hydrochar synthesis through pyrolysis

The pyrolysis process was conducted using a reactor following this method. A total of 8 grams of ironwood waste sample is mixed with 70 mL of deionized water, then the pH of the mixture is adjusted to 1 using H_3PO_4. This mixture is put into a pyrolysis reactor at a temperature of 260 °C for 6 hours. After that, the liquid and solid phases (residue) are separated by vacuum filtration. The solids from pyrolysis, called hydrochar, are then dried in an oven at 105 °C for 2-3 hours.

2.4. Hydrochar activation

Hydrochar was activated using HCl, with a ratio of Hydrochar and activator of 1:10 (w/v). A total of 10 grams of Hydrochar was ground and weighed, then soaked in 100 mL of 1M HCl solution for 24 hours. After that, the sample was filtered and washed until it reached a neutral pH. The residue obtained was then dried in an oven at 110 °C for 3 hours. This residue is activated carbon produced from the activation process.

2.5. Determination of liquid waste preparation

The liquid waste sample utilized in this study was collected from the Jl. Mahir Mahar River, Palangka Raya City, Central Kalimantan Province, employing the grab sampling method. To eliminate particulate matter and potential interfering analytes, the sample was filtered immediately upon collection. Prior to the adsorption experiments, an initial characterization of the wastewater was conducted, which included the determination of Hg(II) concentration via AAS and pH measurement to assess its acidity level.

2.6. Optimum batch adsorption conditions

To determine the optimal conditions for the batch adsorption process, three key parameters were evaluated: pH variation, contact time, and adsorption isotherm analysis. The effect of the matrix on liquid waste samples was also examined using the spike technique, with $HgCl_2$ solution serving as the Hg(II) source.

The effect of pH on adsorption efficiency was assessed by adding 1 g of activated carbon adsorbent to 100 mL of liquid waste with pH values adjusted to 3, 5, 7, and 9 using 0.1 M NaOH and HCl solutions. The suspensions were agitated at 150 rpm for 60 minutes using a mechanical shaker and subsequently allowed to settle for 15 minutes before filtration. The resulting filtrates were analyzed via AAS to determine the adsorption efficiency (%).

To evaluate the effect of contact time on mercury adsorption, 1 g of the adsorbent was added to 100 mL of liquid waste at the previously determined optimum pH. The mixture was stirred at 150 rpm, with contact times varied at 30, 60, 90, and 120 minutes. After each interval, the suspensions were left to settle for 15 minutes before filtration. The filtrates were analyzed using AAS, and the adsorption efficiency (%) and adsorption kinetics were calculated.

To investigate the adsorption isotherm, the adsorbent mass was varied at 1, 1.5, 2, 2.5, and 3 g, each added to 100 mL of liquid waste at the optimum pH and contact time. The samples were stirred under identical conditions, left to stand for 15 minutes, and then filtered. The final filtrates were analyzed via AAS, and the adsorption efficiency (%), adsorption capacity, and adsorption isotherm models were evaluated.

2.7. Dynamic adsorption process (fixed-bed column)

A glass tube with 1.5 cm in diameter and 20 cm in height was used to construct the column reactor. Activated carbon adsorbent was inserted into the column and compacted using a spatula. Glass wool will be added to the top and bottom of the adsorbent in the column. The liquid waste sample will use the optimum pH that has been tested in the batch adsorption process. The adsorption process lasts for 24 hours, with effluent sampling every 60 minutes. The effluent will be tested using AAS. Dynamic adsorption system (fixed bed column) will be used, and the removal percentage (%) and adsorption kinetics are calculated using Thomas and Bohart-Adam models.

3. RESULTS AND DISCUSSION

3.1. Pyrolysis and acid activation of ironwood-based activated carbon

The synthesis of activated carbon involves pyrolysis as an initial step, wherein organic precursors are subjected to high temperatures (400–800 °C) under anoxic conditions. This thermal decomposition process volatilizes organic compounds, yielding a porous carbonaceous solid with a well-defined microstructure. The resulting carbon material, typically characterized by macro and mesopores, possesses a relatively low surface area, necessitating further activation to enhance its adsorption properties (Ioannidou & Zabaniotou, 2007).

To improve porosity and surface functionality, acid activation was employed using phosphoric acid (H_3PO_4) and sulfuric acid (H_2SO_4). Acid treatment promotes pore expansion and the formation of new adsorption sites, thereby augmenting the adsorption capacity of the carbon matrix. Additionally, acid activation enhances the hydrophobic nature of the material, improving its efficiency in sequestering non-polar organic compounds and metal contaminants from aqueous media (Tseng, 2006). This modification is critical for optimizing the carbon's performance in heavy metal removal applications.

3.2. Adsorption performance and mercury removal efficiency

The adsorption capability of ironwood-derived activated carbon for mercury removal was evaluated under varying experimental conditions. Batch adsorption studies demonstrated a direct correlation between the mass of activated carbon and the reduction in mercury concentration. The results indicated that increasing the adsorbent dosage led to enhanced mercury sequestration, reflecting the material's high adsorption efficiency.

At an initial adsorbent dose of 0.1 g, the residual mercury concentration in solution was measured at 5.157 ppm, corresponding to an adsorption efficiency of 86.23%. As the adsorbent mass was progressively increased to 0.7 g, the mercury concentration decreased significantly to 1.306 ppm, achieving a maximum adsorption efficiency of 96.53%. The highest recorded adsorption capacity was 36.163 mg/g, underscoring the strong affinity of ironwood-based activated carbon for mercury uptake. These findings highlight the potential of acid-activated ironwood as a viable adsorbent for heavy metal remediation, demonstrating its effectiveness in aqueous mercury removal applications.

3.3. Effect of pH on mercury adsorption efficiency

The impact of pH on mercury adsorption efficiency was investigated by varying the pH from 1 to 4. The experimental results indicate that pH plays a critical role in the adsorption process, influencing the interaction between mercury ions and the activated carbon surface. At pH 1, the highest adsorption was observed, with an adsorbed mercury concentration of 38.19 ppm. As the pH increased to 2, the

adsorbed mercury concentration slightly decreased to 35.31 ppm, suggesting a decline in adsorption efficiency. A further reduction was recorded at pH 3, where the adsorbed mercury concentration was 35.05 ppm, followed by a slight increase to 36.15 ppm at pH 4.

The adsorption behavior across different pH levels is depicted in **Figure 2**, which demonstrates fluctuations in adsorption efficiency as a function of pH. These variations highlight the importance of maintaining an optimal pH level for effective mercury removal. The maximum adsorption was achieved at pH 1, indicating that lower pH conditions facilitate stronger interactions between mercury ions and the activated carbon surface.

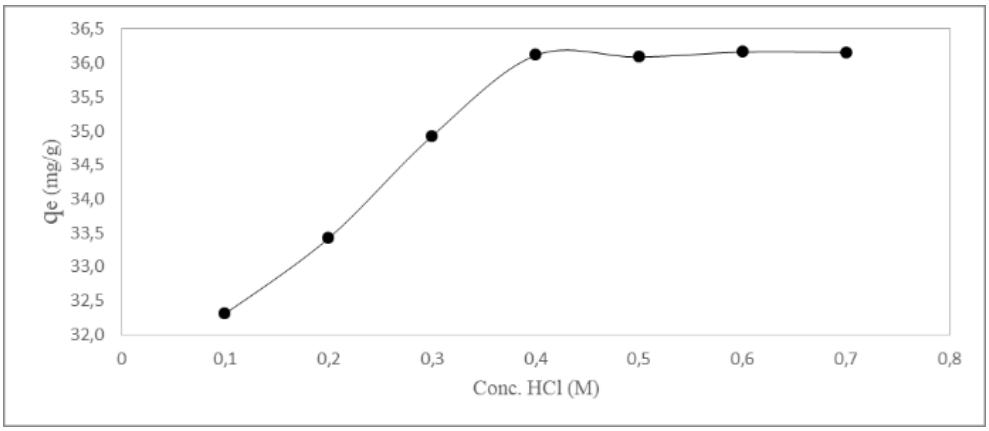

Figure 1. Effect of HCl concentration on Ironwood activated carbon

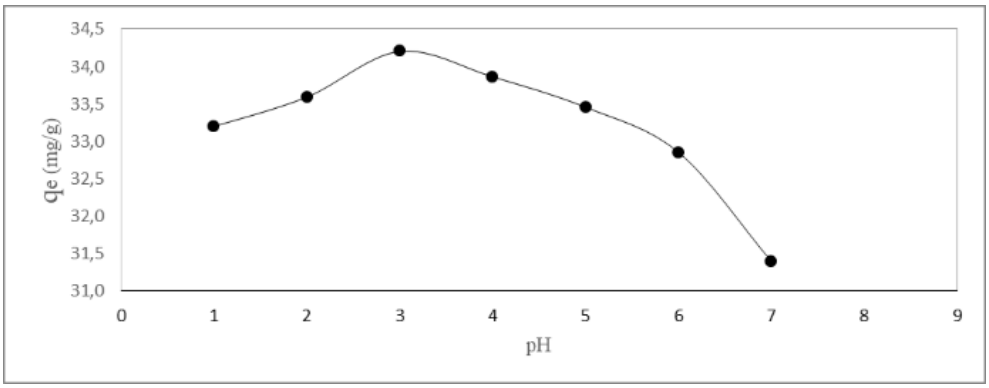

Figure 2. Impact of pH on the adsorption capacity of Ironwood activated carbon

3.4. Effect of contact time on mercury adsorption

To evaluate the influence of contact time on adsorption efficiency, experiments were conducted with varying contact durations ranging from 20 to 100 minutes. The results revealed that adsorption efficiency increased with contact time until equilibrium was reached. At 20 minutes, the remaining mercury concentration was 4.99 ppm, corresponding to an adsorption efficiency of 86.97%. As contact time increased to 40 minutes, the remaining mercury concentration decreased to 2.77 ppm, with an adsorption efficiency of 92.75%. The trend continued, reaching 94.31% adsorption efficiency at 80 minutes (2.18 ppm mercury concentration). However, after 100 minutes, the efficiency plateaued at 94.59%, with a final mercury

concentration of 2.07 ppm, indicating equilibrium had been established.

The adsorption capacity also increased with contact time, reaching a maximum of 36.26 mg/g at 100 minutes (**Figure 3**). These results suggest that activated carbon exhibits high mercury-binding efficiency, particularly during the initial adsorption phase, before approaching saturation.

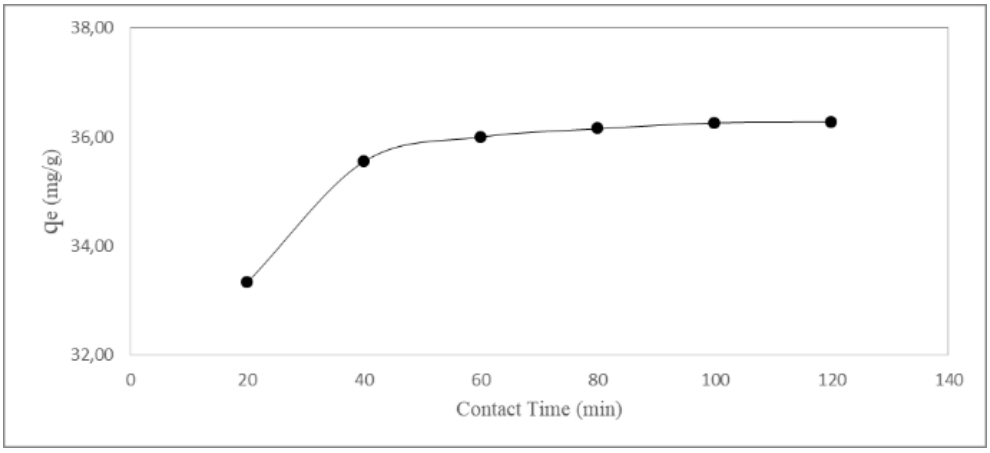

Figure 3. Impact of contact duration on the adsorption capacity of Ironwood activated carbon

3.5. Adsorption kinetics analysis

The adsorption kinetics were analyzed using both first-order and pseudo-second-order models to determine the mechanism governing mercury uptake. The experimental data exhibited a stronger correlation with the pseudo-second-order kinetic model, as demonstrated by the linear relationship in **Figure 4**. The correlation coefficient (R^2) for the pseudo-second-order model exceeded 0.9998, while the first-order model exhibited a significantly lower fit (R^2 = 0.1104). This suggests that the adsorption process is predominantly controlled by chemisorption, where chemical interactions between mercury ions and functional groups on the activated carbon surface dictate the adsorption rate.

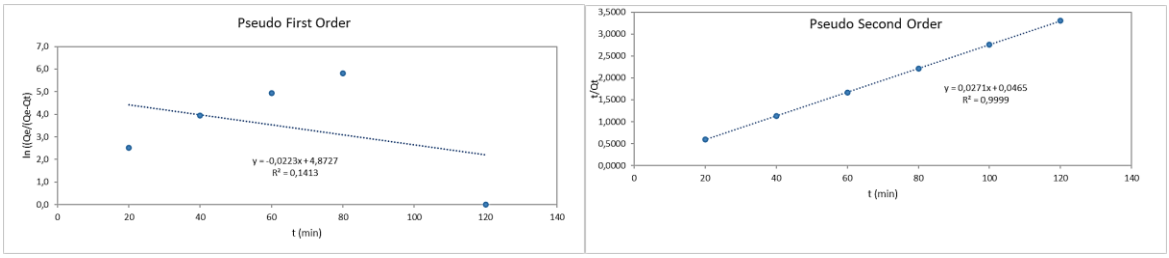

(a) (b)

Figure 4. Linear fitting representing (a) pseudo-first-order and (b) second-order kinetics of mercury adsorption

The adsorption mechanism follows a chemisorption model, further supported by the kinetic rate dependency on the square of mercury concentration, expressed as $(q-q)et^2$. The kinetic parameters obtained for the adsorption process are presented in **Table 1**. These findings reinforce the hypothesis that activated carbon adsorption of mercury is a chemically driven process rather than purely physical interaction.

3.6. Effect of mercury concentration on adsorption capacity

The adsorption behavior of mercury onto ironwood-derived activated carbon was evaluated by varying the initial mercury concentration. As depicted in **Figure 5**, the adsorption capacity exhibited a distinct trend as a function of mercury concentration. At lower concentrations (<500 ppm), the adsorption process proceeded at a relatively slow rate, likely due to the availability of a substantial number of unoccupied active sites on the adsorbent surface. This condition allowed nearly complete adsorption of the available mercury ions, resulting in a lower overall adsorption rate.

Conversely, at higher mercury concentrations (>500 ppm), the adsorption process reached a plateau, indicating saturation of the available active sites on the adsorbent. As the adsorption sites became fully occupied, no additional mercury ions could be effectively adsorbed, thereby leading to an equilibrium state. The findings suggest that mercury adsorption onto ironwood-activated carbon achieved a maximum capacity at approximately 500 ppm before gradually declining as the concentration increased further. This decline may be attributed to the limited availability of additional adsorption sites or potential repulsive interactions between the adsorbed mercury ions and those remaining in the solution.

Tabel 1. Adsorption kinetic model for mercury

Material	Pseudo 1st Order		Pseudo 2nd Order	
	β (menit-1)	R^2	K_2 (g/mg.menit)	R^2
Ironwood activated carbon	0,0204	0,9998	0,01712	0,1104

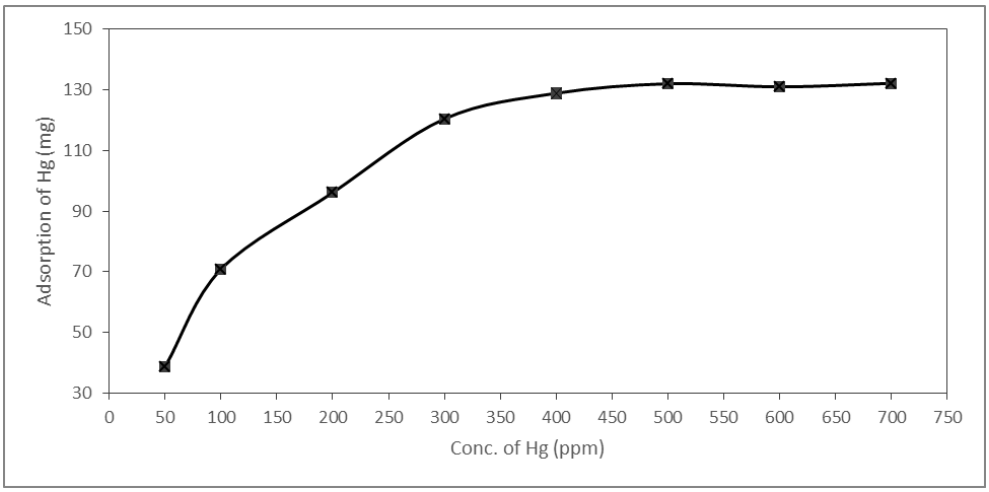

Figure 5. Effect of mercury concentration on the adsorption capacity of Ironwood activated carbon

3.7. Adsorption isotherm modeling

To gain deeper insights into the adsorption mechanism, the equilibrium adsorption data were analyzed using the Langmuir and Freundlich isotherm models. Adsorption equilibrium, which governs adsorption energy and capacity, is described by these isotherm models, illustrating the relationship between the amount of mercury adsorbed and its residual concentration in solution. The results of the model fitting are presented in **Figure 6**.

The correlation coefficient (R^2) was employed to assess the suitability of each model in describing the experimental data. The Freundlich isotherm model exhibited a correlation coefficient of R^2 = 0.9519, indicating moderate agreement with the data. However, the Langmuir model provided a significantly better fit, with R^2 = 0.999, suggesting a high degree of consistency with the experimental results. The superior fit of the Langmuir model implies that mercury adsorption onto ironwood-activated carbon occurs predominantly as a monolayer on a homogenous surface, with uniform adsorption energy across all sites.

Based on these findings, the adsorption process is likely governed by chemisorption or strong electrostatic interactions between the mercury ions and the functional groups present on the adsorbent surface. The equilibrium adsorption parameters derived from both isotherm models are summarized in **Table 2**, further confirming that the Langmuir model provides a more accurate description of the adsorption behavior. These results showed the effectiveness of ironwood-activated carbon as a potential adsorbent for mercury removal, with adsorption characteristics that align well with monolayer adsorption principles. Future studies could explore the influence of additional factors, such as temperature and competing ions, to further optimize the adsorption process for practical applications in wastewater treatment.

The adsorption capacity (B) of mercury on the Ironwood activated carbon composite can be calculated using the Langmuir isotherm model, as shown in Table 2. The adsorption capacity (B) of the Ironwood activated carbon composite is 4.372 x 10^{-4} mol/g for mercury. The adsorption energy is calculated using the Langmuir isotherm model with the formula E = RT ln K. The calculation results show that an energy of 26.64 kJ/mol is required for the adsorption of mercury on the Ironwood activated carbon composite. This indicates the presence of electrostatic interactions between the adsorbent and mercury. Since mercury is positively charged and the active sites of the Ironwood activated carbon composite are also positively charged, an electrostatic bond is formed between the two.

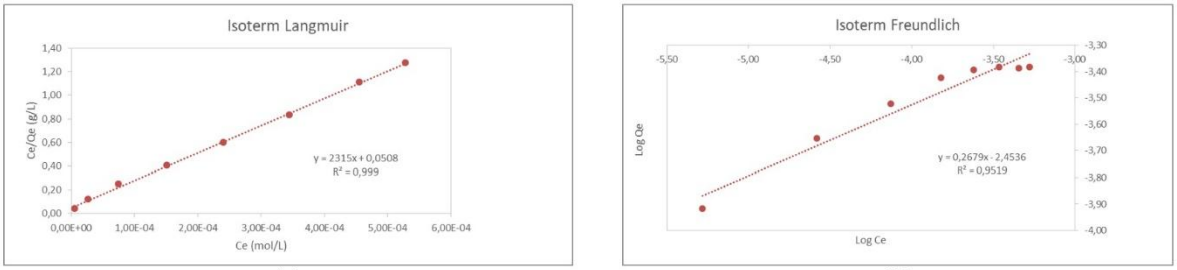

(a) (b)

Figure 6. Linearized adsorption isotherm curve for mercury adsorption adsorbent. (a) Langmuir model and (b) Freundlich model

Tabel 2. Equilibrium kinetic model for mercury

Material	Adropsi Langmuir				Adsorpsi Freundlich		
	B (mg/g)	K (L/mol)	E (kJ/mol)	R^2	B (mg/g)	N	R^2
Ironwood activated carbon	4,372 x 10^{-4}	48558,39	26,64	0,9992	3,574 x 10^{-3}	3,743	0,9456

4. CONCLUSIONS

The study confirmed the successful synthesis of ironwood-based activated carbon, which demonstrated high efficiency in mercury adsorption. Activation of the adsorbent using HCl acid was proven to significantly increase the mercury adsorption efficiency. The optimum pH value found was pH 1, where high hydrogen ions (H^+) increased the interaction between mercury and active sites on the adsorbent surface, resulting in maximum adsorption efficiency. In addition, the optimum contact time for mercury adsorption was achieved at 80 minutes, after which the adsorption process reached equilibrium and did not show a significant increase in mercury absorption. The adsorption kinetics data showed that this process followed a second-order kinetic model, with an adsorption rate of 0.017119 g/mg.min, which was more in accordance with the experimental results compared to the first-order model. The optimum mercury concentration for adsorption was around 500 ppm, where the maximum adsorption capacity was achieved before the process reached equilibrium. The Langmuir isotherm model best fit the data, with an adsorption capacity of 63.036 mg/g, suggesting strong electrostatic interactions between mercury and the adsorbent.

ACKNOWLEDGMENT

The authors would like to express their deepest gratitude to all those who contributed to the successful completion of this research. We also wish to extend our appreciation to LPPM Palangka Raya University for their financial support and resources, which made this work possible. Additionally, the authors would like to acknowledge the valuable feedback from the reviewers and editorial team, whose constructive comments significantly enhanced the quality of this paper. Finally, a heartfelt thanks to our families and colleagues for their continued support and patience throughout the research process.

LIST OF REFERENCES

Hananingtyas, I. (2017). Bahaya Kontaminasi Logam Berat Merkuri (Hg) Dalam Ikan Laut. *Jurnal Teknik Lingkungan*, *2*(2), 38–45.

Baroya, U. B. A., Mahdie, M. F., & Thamrin, G. A. R. (2023). Uji ketahanan kayu ulin (*Eusideroxylon Zwageri*), bengkirai (*Shorea Laevifoia Endert*), dan meranti merah (*Shorea Leprosula Miq*) sebagai bahan baku pembuatan perahu terhadap organisme perusak kayu. 06(1), 170–176.

Harmono, H. D. (2020). Validasi Metode Analisis Logam Merkuri (Hg) Terlarutn pada Air Permukaan dengan Automatic Mercury Analyzer. Indonesian Journal of Laboratory, 2(3), 11. https://doi.org/10.22146/ijl.v2i3.57047

Hidayat, A., & Nasution, R. (2018). Adsorpsi Logam Berat Timbal (Pb) dengan Karbon Aktif dari Tempurung Kelapa. Jurnal Pengolahan Lingkungan, 5(2), 101-115

Ioannidou, O., & Zabaniotou, A. (2007). Agricultural residues as precursors for activated carbon production—A review. Renewable and Sustainable Energy Reviews, 11(9), 1966-2005.

Miftahurrahmah, Suhendrayatna, & Muhammad Zaki. (2017). Penyisihan ion logam merkuri (Hg^{2+}) menggunakan adsorben berbahan baku limbah pertanian dan gulma tanaman. Jurnal Teknik Kimia USU, 6(1), 7–11. https://doi.org/10.32734/jtk.v6i1.1558

Mursyidin, Dindin H. 2006. Menanggulangi Pencemaran Logam Berat. Yayasan Cakrawala Hijau Indonesia. Dosen Biologi FMIPA Unlam Banjarbaru.

Nafilah, S., & Noor, R. (2021). Aplikasi Karbon Aktif Kayu Ulin sebagai

Adsorben dalam Menurunkan Bahan Organik Alami (BOA) pada Air Gambut. Jernih: Jurnal Tugas Akhir Mahasiswa, 4(1), 1-12.

Oko, Syarifuddin, et al (2020). "Pemurnian Minyak Jelantah dengan Metode Adsorbsi Menggunakan Arang Aktif dari Serbuk Gergaji Kayu Ulin (Eusideroxylon Zwageri)." Jurnal Riset Teknologi Industri, Dec. 2020, pp. 124-132, doi:10.26578/jrti.v14i2.6067.

Ramanda, Y., & Sukadana, I. W. (2020). Pemanfaatan Karbon Aktif dari Serbuk Gergaji untuk Adsorpsi Merkuri pada Limbah Tambang. Jurnal Teknologi Lingkungan, 7(3), 45-60.

R. Henti Hendalastuti, & Siregar, I. Z. (2007). KERAGAMAN GENETIK DAN UPAYA KONSERVASI ULIN (Eusideroxylon zwageri) DI INDONESIA. ITTO Workshops Proceedings, May 9th, 2007. Bogor, West Java, 7(3), 213–221.

Sudarmaji, Corie Indria Prasasti., J. M. (2006). Toksikologi Logam Berat B3 Dan Dampaknya Terhadap Kesehatan. Jurnal Kesehatan Lingkungan, 2(23), 129–142. https://www.neliti.com/publications/3956/toksikologi-logam-berat-b3-dan-dampaknya-terhadap-kesehatan

Tseng, R. L. (2006). Physical and chemical activation of corn cob-based carbon for carbon dioxide adsorption. Journal of Hazardous Materials, 147(3), 1020-1027.

Yudi, F., & Itta, D. (2014). Sistem Pengelolaan dan Peredaran Kayu Ulin (Eusideroxylon zwageri T. et. B) dari Hutan Alam di Kalimantan Selatan.

Jurnal Ilmiah Berkala: Sains dan Terapan Kimia
Vol. 19 No. 1, Januari 2025

Synthesis And Characterization Of Acid-Activated Sago Dregs Biochar And Testing Its Ability As An Adsorbent For Rhodamine B Dyes

Sintesis Dan Karakterisasi *Biochar* Ampas Sagu Teraktivasi Asam Serta Uji Kemampuannya Sebagai Adsorben Zat Warna *Rhodamine B*

Musa Habib[1], Dahlena Ariyani[2], Ahmad Budi Junaidi[3]

[1]Laboratory of Biomaterial Chemsitry, Faculty of Matematics and Natural Science, Lambung Mangkurat University, Banjarbaru, 70714, Indonesia
[2]Departement of Chemsitry, Faculty of Matematics and Natural Science, Lambung Mangkurat University, Banjarbaru, 70714, Indonesia

Email: *dariyani@ulm.ac.id*

ABSTRACT

Synthesis & characterization of acid-activated sago pulp biochar as an adsorbent of rhodamine B dye has been carried out. This study aims to synthesize & characterize sago pulp biochar activated with HCl 1 M & H_3PO_4 0,214 M solutions & to assess its ability as an adsorbent of rhodamine B dye. This biochar is produced through a pyrolysis method with a combustion temperature of 700 °C for 2 hours. The results of the pyrolysis biochar were then activated with HCl 1 M & H_3PO_4 0,214 M acid solvents & then analyzed the effect of contact time, pH, & initial concentration on its ability to adsorb rhodamine B dye. Characterization using Fourier Infrared (FTIR) showed the presence of alkene groups & aromatic groups (C=C) & bonds (C−O) & (C−C) which play an important role in the adsorption process. The results of the water content of BAS, BAS/HCl & BAS/H3PO4 produced were 2.57%, 4.47% & 5.06% which met the requirements of SNI 06-3730-1995. The results of the surface area test showed BAS/H_3PO_4 with the largest surface area of 0,520 m^2/g & BAS of 0,452 m^2/g while the smallest surface area was BAS/HCl of 0,445 m^2/g. The study of the effect of pH & contact time on the adsorption capacity of rhodamine B showed that the optimum adsorption capacity of pure sago pulp biochar (BAS) at neutral pH with a contact time of 15 minutes, BAS/HCl at acidic pH with a contact time of 180 minutes, & BAS/H_3PO_4 at alkaline pH with a contact time of 60 minutes. Based on the analysis results, the adsorption process of rhodamine B on biochar follows the Langmuir & Freundlich isotherms with maximum adsorption capacities for BAS, BAS/HCl, & BAS/H_3PO_4 of 4.285 mg/g, 4.834 mg/g, & 3.934 mg/g, respectively.

Keywords: biochar, sago pulp, adsorption, rhodamine B

ABSTRAK

Sintesis dan karakterisasi biochar ampas sagu teraktivasi asam serta uji kemampuannya sebagai adsorben zat warna rhodamine B telah dilakukan. Penelitian ini bertujuan untuk mensintesis dan mengkarakterisasi biochar ampas sagu yang diaktivasi dengan larutan HCl 1 M dan H_3PO_4 0,214 M serta mengkaji kemampuannya sebagai adsorben zat warna rhodamine B. Biochar dihasilkan melalui metode pirolisis dengan suhu pembakaran 700 °C selama 2 jam. Hasil biochar pirolisis kemudian diaktivasi dengan pelarut asam HCl 1 M

dan H_3PO_4 0,214 M kemudian di analisis pengaruh waktu kontak, pH, dan konsentrasi awal terhadap kemampuannya dalam mengadsorpsi zat warna rhodamine B. Karakterisasi menggunakan Fourier Infrared (FTIR) menunjukkan adanya gugus alkena dan gugus aromatik (C=C), ikatan (C−O) dan (C−C) yang berperan penting dalam proses adsorpsi. Hasil analisis kadar air BAS, BAS/HCl dan BAS/H_3PO_4 berturut-turut sebesar 2,57%, 4,47% dan 5,06% (telah memenuhi syarat SNI 06-3730-1995). Hasil uji adsorpsi dengan mengunakan metilen biru menunjukkan bahwa BAS/H_3PO_4 memiliki luas permukaan paling besar yaitu 0,520 m^2/g dan BAS sebesar 0,452 m^2/g sedangkan luas permukaan paling kecil yaitu BAS/HCl sebesar 0,445 m^2/g. Kajian pengaruh pH dan waktu kontak terhadap kemampuan adsorpsi rhodamine B menunjukkan bahwa kemampuan adsorpsi optimum biochar ampas sagu murni (BAS) pada pH netral dengan waktu kontak 15 menit, BAS/HCl pada pH asam dengan waktu kontak 180 menit, dan BAS/H_3PO_4 pada pH basa dengan waktu kontak 60 menit. Berdasarkan hasil analisis, proses adsorpsi rhodamine B pada biochar mengikuti isoterm Langmuir dan Fruendlich dengan kapasitas adsorpsi maksimum untuk BAS, BAS/HCl, dan BAS/H_3PO_4 berturut-turut sebesar 4,285 mg/g, 4,834 mg/g, dan 3,934 mg/g.

Kata kunci: biochar, ampas sagu, adsorpsi, rhodamine B.

Received: 03 February 2025; **Accepted**: 30 December 2024: **Available online**: 30 January 2025

1. INTRODUCTION

Water pollution is a major problem with serious implications for human life and ecosystems. Water pollution caused by dyes, especially Rhodamine B, is one of the most urgent environmental problems to be addressed. Rhodamine B is a synthetic dye that is widely used in the textile industry and has carcinogenic and toxic properties, so it can have a serious impact on human health and aquatic ecosystems (Mahardiani et al., 2024). Waste containing Rhodamine B are often discharged into the environment without adequate treatment, resulting in the accumulation of this hazardous substance in the environment. Therefore, an effective and environmentally friendly method to remove the dye is needed.

An interesting approach to dye wastewater treatment is the use of biochar-based adsorbents in the adsorption process. Biochar is a carbon material obtained from the pyrolysis of biomass at high temperatures under low oxygen conditions, such as wood and fibers (Rusdi et al., 2023). Biochar from sago pulp has the potential to be a sustainable solution in waste management because it can be activated with acid solvents to increase its adsorption capacity. The activation process of biochar aims to increase the surface area and add active functional groups to its surface. Activation with acids, such as HCl and H_3PO_4, has been shown to increase the surface area and adsorption capacity of biochar, resulting in a higher adsorption capacity of biochar.

Pemakuan village, located in Sungai Tabuk subdistrict, Banjar Regency, South Kalimantan, is the center of the sago industry, which produces large amounts of sago pulp waste. Only about 48% of the starch can be extracted, while the rest is in the form of pulp that is not optimally utilized (Istikowati et al., 2021). Sago pulp is a by-product of the sago starch production process that has the potential to be processed into biochar, thus contributing to waste management and environmental sustainability (Witno et al., 2024). Based on this, it is necessary to study the synthesis and characterization of biochar from acid-activated sago pulp as a Rhodamine B dye adsorbent. The characterization of biochar was studied based on the analysis of functional groups, water content, and surface area. The efficiency of biochar as a rhodamine B adsorbent was investigated by studying the effect of contact time, pH effect, and initial rhodamine B concentration.

The data of this study were obtained from rhodamine B dye dissolved in water to simulate industrial wastewater and biochar produced by pyrolyzing sago pulp collected from Pemakuan village area located in Sungai Tabuk subdistrict, Banjar Regency, South Kalimantan. Biochar characterization was carried out using Fourier Transform Infrared (FTIR) to analyze functional groups. Moisture content analysis was performed using the gravimetric method based on the Indonesian National Standard (SNI) 06-3730-1995. Measurement of absorbance method of the solution was measured using UV-Vis spectrophotometer. Testing the adsorption contact time was done by mixing biochar with 20 ppm Rhodamine B solution at different time intervals, and the absorbance of the filtrate was measured to determine the effectiveness of adsorption. To test the effect of pH on adsorption, rhodamine B solution was used at acidic, neutral and alkaline pH. Then, the adsorption test was carried out with variations in the initial concentration of Rhodamine B solution to determine the adsorption capacity of biochar.

2. MATERIALS AND METHODS

2.1. Materials

The tools used in this research are digital analytical balance (Ohaus), glassware such as goblet glass, watch glass, porcelain cup, glass spoon, glass stirrer, Erlenmeyer, volumetric flask, dropper, volume pipette, desiccator, funnel, glass bottle, spray bottle, shaker (GKL 3005), pH meter, oven; pyrolysis and analytical equipment such as FTIR Spectrophotometer (Shimadzu 8201PC) and UV-Vis Spectrophotometer (Genesys 10v, Thermo Scientific). The materials used in this research are sago pulp biochar with particle size <100 µm, HCl, H_3PO_4, NaOH, Rhodamine B, Methylene Blue, aluminum foil, distilled water and Whatman No. 42 filter paper.

2.2. Methods

This research was conducted at the Laboratory of Enzyme Technology and Biomaterials, Faculty of Mathematics and Natural Sciences, Lambung Mangkurat University Banjarbaru. The preparation of biochar samples using pyrolysis tools was carried out at the Banjarbaru Standardization and Industrial Services Center (BSPJI), the measurement of sample solutions using UV-Vis spectrophotometer was carried out at the Instrument Laboratory of the Faculty of Mathematics and Natural Sciences Banjarbaru, and the identification of sample functional groups using FTIR spectrophotometer was carried out at the Physics Laboratory of the Faculty of Mathematics and Natural Sciences, Lambung Mangkurat University Banjarbaru.

2.2.1 Preparation of Sago Dregs Biochar

The first step taken in this research is to make sago pulp biochar. Making biochar requires the main raw material, namely sago pulp that has been washed and dried until it is free from contaminants. Sago pulp was burned using a pyrolysis tool at 700 °C for 2 hours. A total of 20 grams of sago pulp biochar was then activated by soaking in acid solvents, namely HCl 1 M and H_3PO_4 0.214 M with 500 mL each for 48 hours. After soaking the biochar for 48 hours, the biochar is filtered using filter paper and rinsed with distilled water until the pH is neutral. The neutral sample was then oven dried at 105 °C until constant weight. The resulting sago pulp biochar is then referred to as BAS, and biochar activated with 1 M HCl and 0.214 M H_3PO_4 is then referred to as BAS/HCl and BAS/H_3PO_4.

2.2.2 Moisture content test

A total of 1 gram of sago pulp biochar is put into a porcelain cup that has known weight. The calculation of water content was carried out based on the Indonesian National Standard (SNI) 06-3730-1995 by weighing the weight of the empty

container and weighing the filter paper before use. The cup containing the sample was heated in an oven at 105 °C until constant weight, then cooled in a desiccator, then weighed. The same thing was done repeatedly until the weight was constant.

2.2.3 Surface area measurement

Surface area measurement was conducted using UV-Vis spectrophotometer. Samples of BAS, BAS/HCl and BAS/H_3PO_4 biochar were weighed as much as 0.1 g and then each was added to 20 mL of 100 ppm methylene blue solution. The mixture was shaken for 40 minutes. The solution was filtered and then the filtrate was measured for absorbance using a UV-Vis spectrophotometer. Methylene blue standard solutions with concentrations of 2, 3, 4, 5, and 6 ppm were prepared first to obtain the maximum wavelength and standard curve.

2.2.4 Determination of the optimum wavelength (λ) of Rhodamine B using UV-Vis Spectrophotometer

Rhodamine B solution with a concentration of 3 ppm was prepared, then the optimum wavelength was determined by measuring the absorbance of the solution at a wavelength (λ) of 400-700 nm. The wavelength (λ) that gives the maximum absorbance is recorded as the λ_{max}. Measurements were carried out using a UV-Vis spectrophotometer.

2.2.5 Preparation of Rhodamine B standard curve

Make and prepare rhodamine B solution with concentrations of 1.5; 2; 2.5; 3 and 3.5 ppm. Each solution was measured for absorbance using UV-Vis Spectrophotometer with a maximum wavelength (λ) of 552 nm.

2.2.6 Effect of Rhodamine B adsorption contact time on biochar

Weigh each sago pulp biochar (BAS, BAS/HCl and BAS/H_3PO_4) as much as 0.5 g, then put into Erlenmeyer. A total of 50 mL of 20 ppm rhodamine B solution was put into an Erlenmeyer that already contained sago pulp biochar. The sample was then shaken using a shaker at 120 rpm for 5, 15, 30, 60, 120 and 180 minutes. The sample was then separated by filtering the filtrate using Whatman filter paper no.42 and measured the absorbance using a UV-Vis spectrophotometer.

2.2.7 Effect of pH on the ability of biochar to adsorb Rhodamine B dye

Making a 20 ppm rhodamine B solution with acidic, neutral and alkaline pH variations. Making a pH solution is done by adding HCl to lower the pH and NaOH solution to raise the pH of the solution. Weigh each sago pulp biochar (BAS, BAS/HCl, and BAS/H_3PO_4) as much as 0.5 g, then put into an Erlenmeyer. A total of 50 mL of 20 ppm rhodamine B solution was put into the Erlenmeyer which already contained sago pulp biochar. The sample was then shaken using a shaker at 120 rpm for different times, namely 15 minutes (BAS) 60 minutes (BAS/H_3PO_4) and 180 minutes (BAS/HCl), this was adjusted to the optimum adsorption time in the contact time analysis. The sample was then separated by filtering the filtrate using Whatman no.42 filter paper and measured the absorbance using a UV-Vis Spectrophotometer.

2.2.8 Effect of rhodamine B adsorption capacity on biochar

Rhodamine B solution with concentration variations of 10, 20, 30, 40, 50 and 60 ppm were prepared by diluting the 1000 ppm rhodamine B mother solution. The pH value of each solution is set at the optimum pH analysis. A total of 0.1 grams of BAS, BAS/HCl, and BAS/H_3PO_4 samples were weighed using an analytical balance and put into each Erlenmeyer. Each Erlenmeyer containing the sample was put 50 mL of rhodamine B solution into each Erlenmeyer. The mixture in the Erlenmeyer was shaken using a shaker at a speed of 120 rpm at various times, namely 15 minutes (BAS), 60 minutes (BAS/H_3PO_4) and 180 minutes (BAS/HCl). The sample was then filtered, and the filtrate was

separated using Whatman No. 42 filter paper, then the absorbance was measured using a UV-Vis spectrophotometer.

2.2.8 Moisture content

Determination of biochar moisture content is done by measuring mass changes before and after drying using analytical scales. The data obtained in the form of mass before and after drying, which is then processed using Microsoft Excel to calculate the percent (%) of water content in biochar. The calculation of moisture content uses the following equation:

$$\text{Moisture content \%} = \frac{\text{Initial-Final}}{\text{Initial}} \times 100\%$$

Description:
Initial: weight before heating (g)
Final: weight after heating (g)

2.2.9 Biochar surface area

The surface area of biochar was determined from the amount of methylene blue adsorbed, using the equation:

$$S = \frac{\frac{Ca}{m} \times N \times a}{M}$$

Where,

S = adsorbent surface area (m^2/g)
Ca = amount of adsorbed dye (mg)
m = weight of adsorbent (g)
N = avogadro number (6.02×10^{23} particles/mol)
a = size of 1 molecule of methylene blue adsorbate (197×10^{-20})
M = molecular weight of methylene blue (320.5 g/mol)

2.2.10 Adsorption of dyes

The process of dye adsorption by biochar was analyzed using a UV-Vis Spectrophotometer at a wavelength of 552 nm. The measurement results are in the form of absorbance values which will be converted using Microsoft Excel into concentration values and to determine the percent (%) concentration of dyes absorbed by the archite composite. The following calculations were carried out in this study:

$$Ca = Co - Ce$$

Where,

Ca = Concentration of absorbed substances (ppm)
Co = Initial concentration of solution (ppm)
Ce = Residual concentration of dye (ppm)
Determination of the percentage value of dye adsorption on the adsorbent:

$$(\%)\ \text{adsorption} = \frac{Ca}{Co} \times 100\%$$

Data obtained based on parameters such as contact time and optimum pH were made in the form of graphs of the relationship between the percentage of dye adsorption with contact time and the percentage of dye adsorption with optimum pH.

The results of the analysis in procedure 3.5.3 were plotted into the Langmuir (1, 2 and 3) and Freundlich (1, 2 and 3) adsorption isotherm equation graphs to determine the adsorption model on biochar by comparing the greater linearity between the two. The Langmuir isotherm equation graph plots the relationship between Ce/qe and Ce, while the Freundlich equation is the relationship between log qe and log Ce so that a linear equation will be obtained from the two graphs. The optimum adsorption capacity of rhodamine B on biochar (q_{max}) can be obtained from the slope obtained on the plot of Ce/qe against Ce in the Langmuir isotherm equation. Determination of the amount of adsorbate adsorbed:

$$q_e = \frac{Ca\left(\frac{v}{1000}\right)}{m}$$

Where,

qe = amount of adsorbed substance (mg/g)
v = volume of solution (mL)
m = mass of adsorbent (g)

3. RESULTS AND DISCUSSION

3.1 Preparation and Manufacture of Sago Dreg Biochar

The main raw material for making biochar in this study is sago pulp. The sago pulp was first washed and dried to be free from contaminants, then burned by pyrolysis method at a temperature of 700 °C for 2 hours. Pyrolysis is the chemical decomposition of organic materials through a heating process, where the raw material will undergo chemical structural breakdown. This process is a decomposition process through heating with a very limited amount of oxygen (Caturwati et al., 2015). The working principle of pyrolysis involves the decomposition of organic materials through heating at high temperatures in conditions without oxygen or with very limited oxygen. The process starts with drying the material to remove moisture at temperatures below 200 °C. After that, the organic material is further heated to about 200-300 °C, where the decomposition of complex molecules into simpler compounds begins, and light gases are released. Pyrolysis at 300-700 °C causes organic polymer chains to be broken down into gases, liquids, and solids (Herlambang et al., 2020). **Figure 1** is the result of sago pulp biochar before pyrolysis and sago pulp biochar after pyrolysis.

(a) **(b)**

Figure 1. Sago bagasse biochar before pyrolysis (a) and after pyrolysis (b)

In this study, biochar was activated with acid solutions, namely HCl and H_3PO_4. According to research by Arung et al., (2014), hydrochloric acid (HCl) is used as a biochar activator, because hydrochloric acid (HCl) can dissolve impurities so that more pores are formed and the adsorbate absorption process will become more and the selection of H_3PO_4 as an activator because it has thermal stability and can make biochar surface pores more, this is supported by research (Eso, 2021).

3.2 Characterization of sago pulp biochar functional groups using Fourier Transfrom Infrared (FTIR)

Characterization of biochar functional groups using an FTIR spectrophotometer is carried out to identify functional groups present in biochar. FTIR analysis can accurately identify functional groups present in biochar, such as aromatic rings, alcohols, ethers, carboxylic acids, and esters. This is important because functional groups provide information about the chemical structure and properties of biochar (Hidayat, 2021). The following are the results of the FTIR spectra analysis of BAS, BAS/HCl, and BAS/H_3PO_4 show in **Figure 2** and **Table 1**.

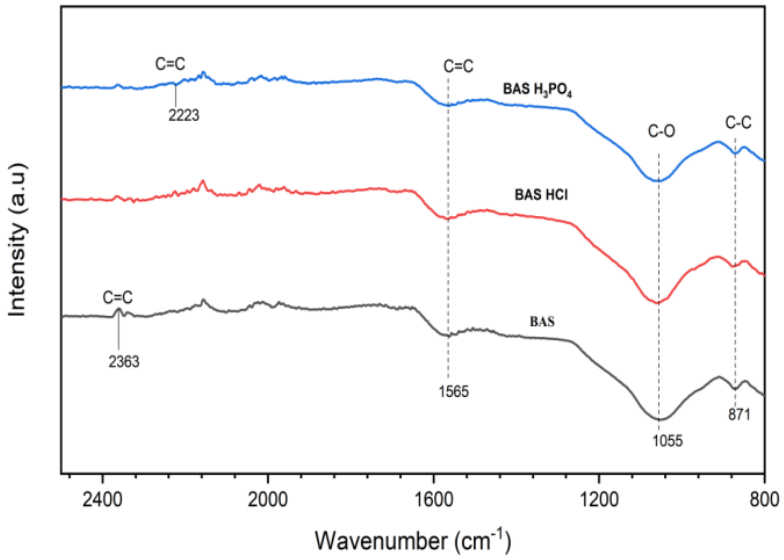

Figure 2. Spectra IR BAS, BAS/HCl, and BAS/H_3PO_4

Tabel 1. Functional groups identification of BAS, BAS/HCl dan BAS/H_3PO_4.

BAS (cm^{-1})	BAS HCl (cm^{-1})	BAS H_3PO_4 (cm^{-1})	Reference Wavelength (cm^{-1})	Functional Group (cm^{-1})
2363		2223	2380-2260	C=C alkena
1565	1565	1565	1540-1640	C=C aromatik
1055	1055	1055	1000-1350	Stretching C−O
871	871	871	666-909	Stretching C−C

Figure 2 shows the results of the FTIR spectra of BAS, BAS/HCl and BAS/H_3PO_4 informing that there are absorption peaks that appear at several wave numbers. The absorption at wave number 2223 cm^{-1} in the BAS/H_3PO_4 sample and wave number 2363 cm^{-1} in the BAS sample, the results of the two samples are in the range of wave numbers 2260-2380 cm^{-1} which is the absorption of aromatic groups (C=C). Absorption at wave number 1565 cm^{-1} as absorption of aromatic groups (C=C) in BAS/HCl (Sartika et al., 2014). Absorption at wave number 1055 cm^{-1} is a stretching vibration (C−O) (Andiani et al., 2022). The absorption at wave number 871 cm^{-1} is a stretching vibration (C−C) (Deswardani et al., 2020). Based on the spectra results, there are several shifts at wave numbers 2400 to 800 cm^{-1} which may be due to the delocalization of double bonds or the occurrence of addition reactions by acid solutions during biochar activation. Activation with acid solutions such as HCl or H_3PO_4 can cause addition reactions, where acid molecules interact with biochar this can produce new bonds such as stretching vibrations.

3.2 Determination of Moisture Content

Determination of water content was carried out by gravimetric method. A total of 1 g of sago pulp biochar is put into a porcelain cup that has known weight. The calculation of water content refers to the Indonesian National Standard (SNI) 06-3730-1995) The value of moisture content shows in **Figure 3**.

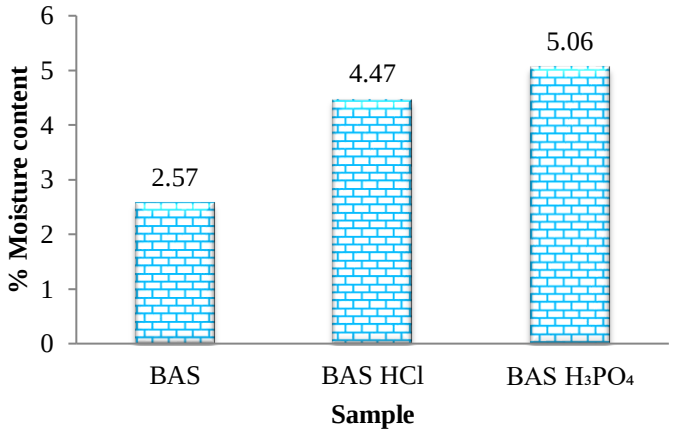

Figure 3. Moisture content value of BAS, BAS/HCl dan BAS/H_3PO_4

Figure 3 shows that activation can increase the water content contained in biochar. Verayana & Iyabu (2018), mentioned that activation with HCl and H_3PO_4 produced biochar with better porosity. Activation with acid solvents can interact with polar functional groups present on the biochar surface. This interaction allows the formation of hydrogen bonds between water molecules. The strong force of attraction between water molecules and atoms that have positive or negative partial charges, thus increasing the ability of biochar to hold moisture and allowing more water molecules to bond to biochar (Tungadi, 2020). Based on the above data, the moisture content in biochar and activated biochar has met the requirements of SNI 06-3730-1995.

3.3 Surface Area

Determination of biochar surface area using methylene blue adsorption method with a wavelength (λ) of 640 nm. This method is the same as that done by Utomo et al. 2019. The results of the biochar surface area analysis can be seen in **Figure 4**.

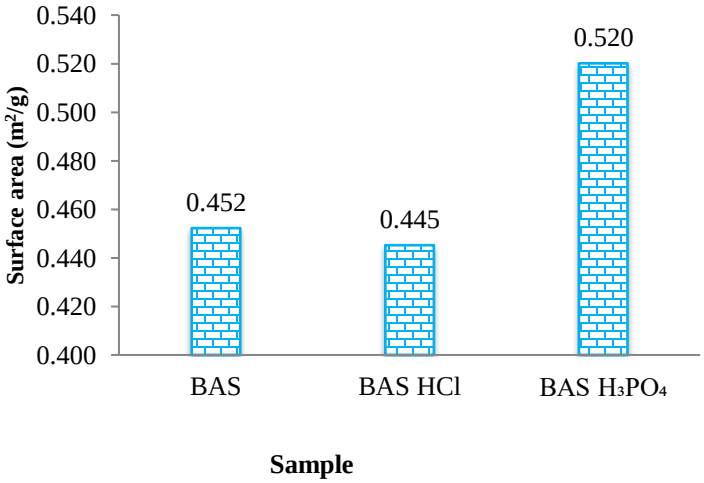

Figure 4. Surface area of biochar

Figure 4 shows that activation with H_3PO_4 can increase the surface area of biochar. There are three processes that occur during activation with H_3PO_4, namely (1) the opening of previously

closed pores, (2) the opening of new pores, and (3) the expansion of existing pores (Harlianingtyas et al., 2023). Some of these things cause the surface area to increase. This increase in surface area corresponds to the increase in water content in H_3PO_4-activated biochar. **Figure 4** also shows a decrease in the surface area of biochar activated with HCl. This can occur because HCl is classified as a strong acid that can cause decomposition in biochar organic matter resulting in damage to the biochar structure (Sulistyorini, 2015).

3.4 Effect of contact time on adsorption of rhodamine B on BAS

The effect of contact time in the adsorption process of rhodamine B dye on biochar is an important aspect in studying adsorption efficiency. The contact time test involves the adsorption process between adsorbent and adsorbate. Analysis of the effect of contact time aims to determine the length of time needed to adsorb the solution until it reaches equilibrium. Adsorption equilibrium is reached when the amount of substance adsorbed on the surface of the adsorbent is saturated so that it becomes constant, which means that there is no longer a change in the concentration of solute in solution or on the surface of the adsorbent (Atok et al., 2024). Analysis of the effect of contact time on rhodamine B adsorption on each type of biochar (BAS, BAS/HCl and BAS/H_3PO_4) was carried out at a variety of contact times, namely 5, 15, 30, 60, 120 and 180 minutes. The results are shown in **Figure 5**.

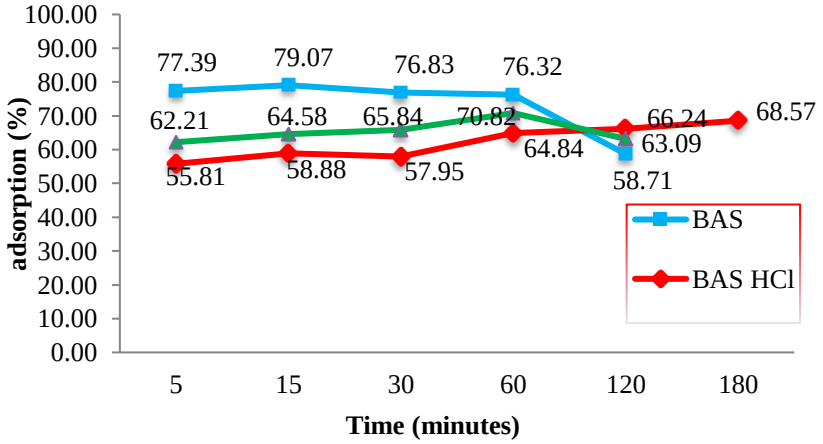

Figure 5. Relationship between contact time and percentage adsorption of rhodamine B dye on biochar

Figure 5 shows that the high percentage of adsorption is influenced by the type of sago pulp biochar and contact time until it reaches equilibrium time. The results showed that the optimum adsorption ability of BAS was 79.07% with a contact time of 15 minutes, BAS/HCl was 68.57% with a contact time of 180 minutes and BAS/H_3PO_4 was 70.82% with a contact time of 60 minutes. These results indicate that the adsorbent has reached saturation point.

Adsorption equilibrium is a condition in which all active sites on the adsorbent surface have been filled by the adsorbate, so that the adsorption state has reached a maximum or saturation point. After the equilibrium time is reached, there is no more significant increase because the adsorbent surface is saturated with dyes that form a layer so that it covers the adsorbent layer (Kurniawati & Indriyanti, 2021).

Based on the curve in **Figure 5**, too long contact time can cause a decrease in adsorption on BAS and BAS/H_3PO_4, this can occur because the adsorbate can be released back into the solution which indicates the type of interaction between the adsorbent and the adsorbate occurs physically (Aisyahlika et al., 2018). Unlike the case with BAS/HCl, up to 180 minutes there is still an increase in the percentage of adsorption, which indicates that the interaction that occurs between the adsorbent and adsorbate is more stable.

3.5 Effect of pH on the ability of BAS to adsorb rhodamine B dye

The degree of acidity or pH value is a variable that can determine the performance and interaction between compounds. The pH condition in the adsorption process can affect the charge of the adsorbent (biochar) and the adsorbed compound (rhodamine B) in the solution which affects the type of adsorption interaction that occurs. The following is the alleged structure of rhodamine B under various pH conditions, as follows:

In this experiment, the pH variation of rhodamine B dye solution was carried out in acidic (2.92), neutral (7.00), and alkaline (9.71) conditions. The solution before and after adsorption was measured absorbance with UV-Vis spectrophotometer with a wavelength of 552 nm. The results of the study are shown in **Figure 6**.

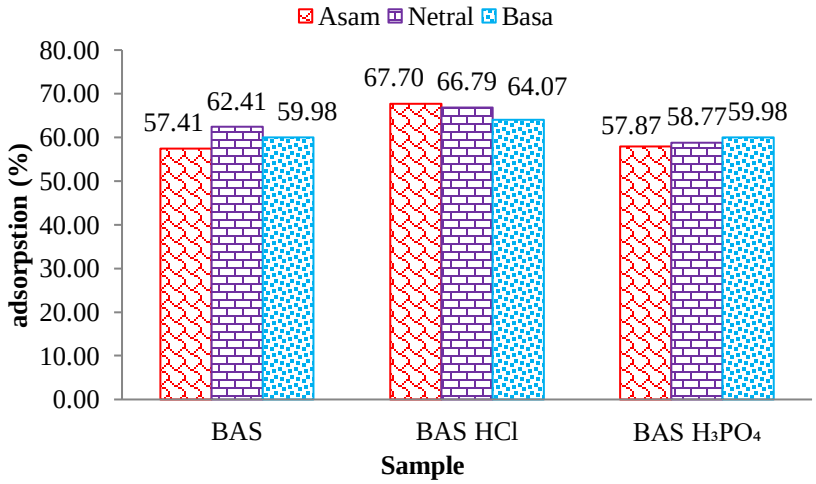

Figure 6. the effect of pH on the adsorption ability of rhodamine B on sago pulp biochar

Based on **Figure 6**, the adsorption percentage of BAS is optimum at neutral pH with adsorption ability of 62.41%, BAS/HCl is optimum at acidic pH with adsorption ability of 67.70% and BAS/H_3PO_4 is optimum at alkaline pH with adsorption ability of 59.98%. However, based on **Figure 6**, the pH of the solution does not have a significant effect on the adsorption ability of biochar.

3.6 Effect of initial concentration of rhodamine B solution on biochar adsorption capacity

Analysis of the effect of initial concentration aims to determine the amount of rhodamine B dye that can be adsorbed on each gram of sago pulp biochar. This analysis was carried out by contacting biochar of 0.1 g BAS, BAS/HCl, and BAS/H_3PO_4 into a solution of rhodamine B dye with a concentration variation of 10, 20, 30, 40, 50 and 60 ppm. The data in **Table 2** shows the amount of rhodamine B absorbed by each gram.

Table 2. The effect of initial concentration of rhodamine B towards biochar adsorption capacity

Variasi konsentrasi *rhodamine B* (ppm)	BAS (mg/g)	BAS/HCl (mg/g)	BAS/H_3PO_4 (mg/g)
10	0,370	0,536	0,806
20	0,318	1,327	0,787
30	1,730	2,630	1,493
40	1,588	3,483	2,109
50	4,265	4,834	3,934
60	0,474	0,995	0,00066

Based on **Tabe1 2**, the initial concentration of rhodamine B solution affects the amount of dye adsorbed on biochar. The higher the initial concentration, the higher the amount of dye adsorbed on biochar up to the initial concentration of 50 ppm. The higher initial concentration causes more rhodamine B molecules in the solution thus triggering a higher adsorption rate, because more rhodamine B molecules are encouraged to move to the biochar surface and occupy active sites on the biochar surface until it reaches the adsorption equilibrium point. However, if the initial concentration exceeds 50 ppm (past the adsorption equilibrium point) there is a decrease in adsorption. This can be caused by rhodamine B molecules that are crowded and interact with each other, thus forming larger aggregates. This interaction will inhibit and slow down the rate of dye diffusion into the biochar pore. Sulistyaningsih, (2021) reported that adding more adsorbate (rhodamine B) will not increase the amount adsorbed, which explains that adsorption has reached a saturation point. The surface of the adsorbent that has been completely filled by rhodamine B molecules and the addition of a high concentration amount will cause desorption, where molecules that have been bound to the surface of the adsorbent will again release or return to the solution, this is supported by research (Agustina et al., 2022).

In this study, the adsorption capacity of BAS, BAS/HCl, BAS/H_3PO_4 reached 4.285 mg/g, 4.834 mg/g, and 3.934 mg/g, respectively. This result does not correspond to the surface area of the absorbent. BAS/H_3PO_4 has the highest surface area, but its adsorption capacity is smaller than BAS without activation. This indicates that activation with H_3PO_4 can produce large porosity with very small pores so that dye molecules with larger molecules cannot be absorbed into the pores. BAS/HCl has a lower surface area, but greater adsorption capacity than biochar without activation. This can be caused by activation with HCl to produce larger pores so that dyes with large molecules can be adsorbed to the adsorbent surface.

The results of Langmuir and Freundlich isotherm adsorption plots of rhodamine B dye on BAS, BAS/HCl and BAS/H_3PO_4 can be seen in **Figures 6**, **Figure 7**, and **Figure 8** below.

The isotherm plot results in **Figure 6** show that the adsorption of rhodamine B on BAS more closely follows the Freundlich isotherm. The isotherm plot results in **Figures 7** and **Figure 8** show that the adsorption of rhodamine B on HCl and H_3PO_4 activated biochar more closely follows the Langmuir isotherm. The Langmuir adsorption isotherm model assumes that the dye only forms a single layer (monolayer) on a homogeneous adsorbent surface. In contrast, the Freundlich adsorption isotherm assumes that additional absorption occurs in the dye layer above the adsorbent surface (multilayer). An illustration of the Langmuir and Freundlich isotherms is shown in **Figure 9**.

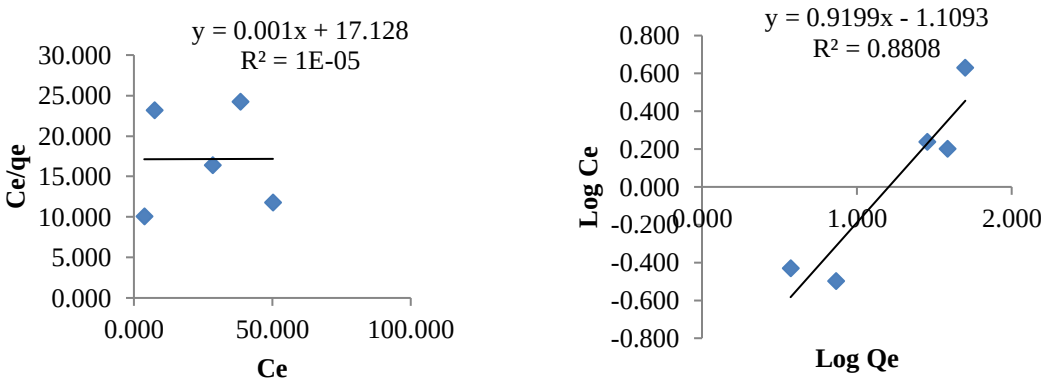

Figure 6. Isotherm plots of (a) Langmuir and (b) Freundlich BAS/against rhodamine B

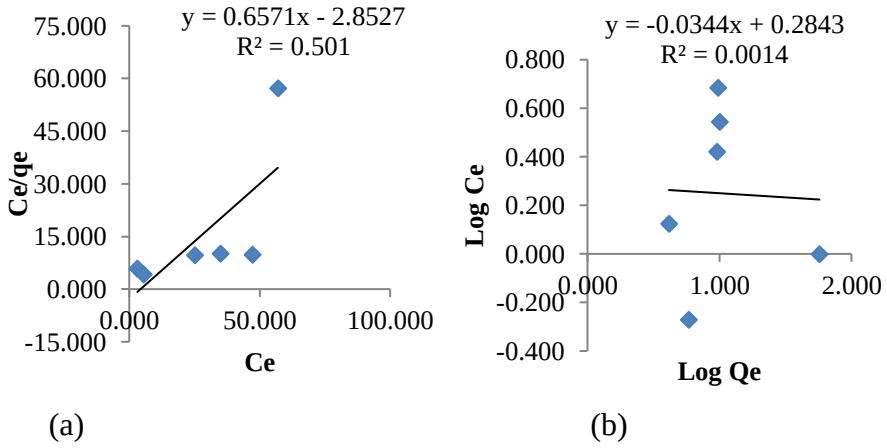

(a) (b)

Figure 7. Isoterm plots (a) Langmuir and (b) Freundlich BAS/HCl against *rhodamine B*

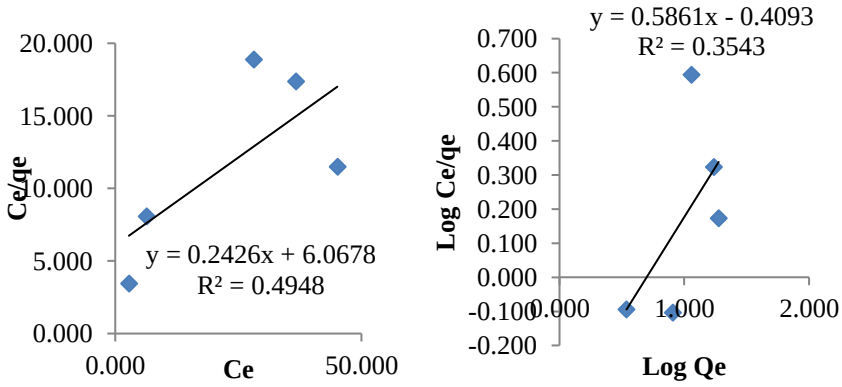

(a) (b)

Figure 8. Isoterm plots (a) Langmuir and (b) Freundlich BAS/H_3PO_4 agains *rhodamine B*

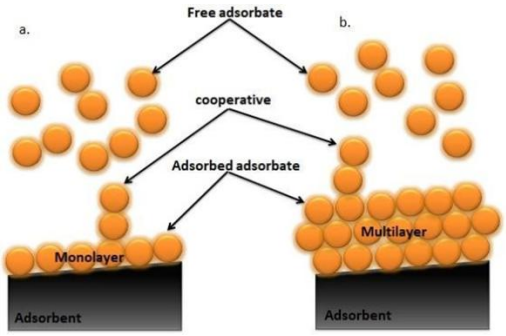

Figure 9. (a) Illustration of the Langmuir adsorption isotherm (b) Illustration of the Freundlich adsorption isotherm (Maryanti et al., 2020).

4. CONCLUSIONS

The conclusion of this research shows that the FTIR spectra of sago dregs biochar shows the presence of functional group absorption peaks from sago dregs as an adsorbent, namely the aromatic ring structure (C=C) and C−O bonds and C−C bonds. The water content of BAS, BAS/HCl, and BAS/H_3PO_4 respectively was 2.57; 4.47; and 5.06% which fulfilled the requirements of SNI 06-3730-1995. The results of surface area analysis show that BAS/H_3PO_4 has the largest surface area, namely 0.520 m^2/g and BAS of 0.452 m^2/g, while the smallest surface area is BAS/HCl of 0.445 m^2/g. The longer the contact time, the greater the adsorption percentage until it reaches equilibrium. BAS reaches optimum at a contact time of 15 minutes with an adsorption percentage of 79.07%, BAS/HCl reaches optimum at a contact time of 180 minutes with an adsorption percentage of 68.57%, and BAS/H_3PO_4 reaches optimum at a contact time of 60 minutes with an adsorption percentage amounting to 70.82%. The optimum adsorption of rhodamine B on BAS occurs at neutral pH with a percentage of 62.41%, BAS/HCl occurs at acidic pH with a percentage of 67.70%, and BAS/H_3PO_4 occurs at alkaline pH with a percentage of 59.98%. The adsorption capacity of biochar without activation reached 4.285 mg/g. The adsorption capacity increased in HCl-activated biochar with an adsorption capacity reaching 4.834 mg/g, while H_3PO_4-activated biochar experienced a decrease in adsorption capacity with an adsorption capacity of 3.934 mg/g.

ACKNOWLEDGMENT

The author would like to thank the Biomaterials Laboratory, Faculty of Mathematics and Natural Sciences, Lambung Mangkurat University for the support provided for this research.

LIST OF REFERENCES

Agustina, L., S. Sitorus & I. Y. L Sari. 2022. Pemanfaatan Arang Aktif Dari Limbah Serbuk Gergaji Kayu Bangkirai (*Shorea Laefivolia* Eudert) Sebagai Adsorben Zat Warna Rhodamin B. Jurnal Atomik. 6 (2) : 119-123.

Aisyahlika, S.Z., M. L. Firdaus & R. Elvia. 2018. Kapasitas Adsorpsi Arang Aktif Cangkang Bintaro (*Cerbera Odollam*) Terhadap Zat Warna Sintetis Reactive RED-120 & Reactive BLUE-198. Alotrop. 2 (2).

Amelia, H., R. Fitria & S. Sunardi. 2023. Kajian Isoterm Adsorpsi Metilen Biru Pada Biochar Kulit Sagu (*Metroxylon Sagu*). Justek: Jurnal Sains Dan Teknologi. 6 (1): 135-142. https://doi.org/10.31764/justek.v6i1.13746

Andiani, B.Y., C. A. Riyanto & Y. Martono. 2022. Characterization Of Cassava (*Manihot Esculenta* Crantz) Peel Activated Carbon Based On Impregnation Ratio And Activation Temperature. Stannum: Jurnal Sains Dan Terapan Kimia. 4 (1): 19-26. https://doi.org/10.33019/jstk.v4i1.2533

Arung, S., M. Yudi & S. Chadijah. 2014. Pengaruh Konsentrasi Aktivator Asam Klorida (HCl) Terhadap Kapasitas Adsorpsi Arang Aktif Kulit Buah Kakao (*Theobroma Cacao*. L.) Pada Zat Warna Methanil Yellow', Al-Kimia, 2(1), Pp. 52-63.

Atok, M.N.L., I. W. B. Suyasa & J. Sibaran. 2024. Peningkatan Performance Arang Aktif Sabut Buah Pinang (*Areca Catechu* L.) Sebagai Adsorben Kation. Jurnal Syntax Admiration. 5 (6): 2182-2195. https://doi.org/10.46799/jsa.v5i6.1230

Caturwati, N. Et Al.2015. Alat Pirolisis Tempurung Kelapa Sawit Sebagai Bahan Baku Briket Biomassa. 1.

Chrisnandari, R.D., W. S. Witasari & A. W. Mustikarini. 2020. Pemanfaatan Karbon Aktif Dari Batang Daun Buah Naga Teraktivasi Asam Kuat Sebagai Adsorben Logam Timbal (Pb). Reka Buana: Jurnal Ilmiah Teknik Sipil Dan Teknik Kimia. 7 (2): 141-158. https://doi.org/10.33366/rekabuana.v7i2.3856

Deswardani, F. Et Al. 2020. Analisis Gugus Fungsi Pada TiO_2/Biochar Dengan Spektroskopi FTIR (Fourier Transform Infrared). Journal Online Of Physics. 5 (2):. 54-58. https://doi.org/10.22437/jop.v5i2.9397

Eso, R. 2021. Efek Variasi Konsentrasi Zat Aktivator H_3PO_4 Terhadap Morfologi Permukaan Dan Gugus Fungsi Karbon Aktif Cangkang Kemiri', Gravitasi. 20 (1): 9-23. https://doi.org/10.22487/gravitasi.v20i1.15519

Harlianingtyas, I. Et Al. 2023. Pembuatan Asap Cair, Biochar, Dan Arang Aktif Dengan Alat Pirolisis Detachable Pada Rintisan Teaching Factory Pembibitan Politeknik Negeri Jember. Agrimas: Jurnal Pengabdian Masyarakat Bidang Pertanian. 2 (2): 97-104.

Herlambang, S. Et Al. 2020. Biochar Salah Satu Alternatif Untuk Perbaikan Lahan Dan Lingkungan.

Hidayat, B.. L.N.A.. & S.T. 2021. Pengaruh Penggunaan Biochar Biomassa Kelapa Sawit Terhadap Aktivitas Mikroorganisme Pada Tanah Ultisol. Jurnal Agro Estate. Jurnal Agro Estate. 5 (1): 14-24. https://doi.org/10.47199/jae.v5i1.77 https://doi.org/10.47199/jae.v5i1.187

Istikowati, W.T., B, Sutiya & S. Sunardi. 2021. Pemanfaatan Limbah Sagu Sebagai Bahan Pakan Ternak Di Desa Pemakuan Laut, Sungai Tabuk, Kabupaten Banjar, Kalimantan Selatan: Utilization Of Sago Waste As Animal Feed Material In Pemakuan Laut Village, Sungai Tabuk, Banjar Regency, South Kalimantan', Pengabdianmu: Jurnal Ilmiah Pengabdian Kepada Masyarakat. 6 (2): 149-155. https://doi.org/10.33084/pengabdianmu.v6i2.1822

Kurniawati, S. & Indriyanti, N.Y. 2021. Adsorption Of Anionic And Cationic Dyes In Batik Wastewater Using Biomass Adsorbents: Literature Review', JKPK (Jurnal Kimia Dan Pendidikan Kimia). 6 (3): 274-291. https://doi.org/10.20961/jkpk.v6i3.55409

Mahardiani, L., S. Saputro.. & W, Ciptonugroho. 2024. Nanopartikel Hematit Termodifikasi Biopolimer (Pemanfaatan Dalam Proses Adsorpsi Dan Fotokatalitik Zat Warna). CV Pajang Putra Wijaya.

Maryanti, R. Et Al. 2020. Adsorption Of Dye On Carbon Microparticles: Physicochemical Properties During Adsorption, Adsorption Isotherm And Education For Students With Special Needs. Sains Malaysiana. 49 (12): 2949-2960. https://doi.org/10.17576/jsm-2020-4912-09

Rusdi., Evizal & E.P. Fembriarti. 2023. Biochar: Pemanfaatan Dan Aplikasi Praktis. Jurnal Agrotropika. 22 (1): 1-12. https://doi.org/10.23960/ja.v22i1.7151

Sartika, N.D. Et Al. 2014. Kajian Pembuatan Arang Aktif Berbahan Baku Bagas Tebu Melalui Kombinasi Proses Karbonisasi Hidrotermal Dan Aktivasi Kimia. Jurnal Teknologi Industri Pertanian. 24 (2).

Sastrohamidjojo, H.1992. Spektroskopi Inframerah. Liberty, Yogyakarta. 3-4.

Sulistyaningsih, T. 2021. Modifikasi Magnetit Menggunakan Asam Humat Guna Meningkatkan Kemampuan Adsorpsi Terhadap Zat Warna Malachite Green. Inovasi Sains Dan Kesehatan. 1.

Sulistyorini, L.D. 2015. Pemanfaatan Kulit Siwalan (*Borassus Flabellifer*) Sebagai Biochar Dengan Pengaruh Konsentrasi Dan Lama Perendaman HCl Pada Proses Aktivasi. Jurnal Bioproses Komoditas Tropis. 3 (2) : 74-80.

Syafitra, D. Et Al. 2020. Pemanfaatan Biochar Dari Sabut Siwalan Sebagai Adsorben Larutan Cu. Chempro. 1 (2) : 1-7. https://doi.org/10.33005/chempro.v1i2.36

Tungadi, R. 2020. Teknologi Nano Sediaan Liquida Dan Semisolida, Buku Ajar.

Utomo, W.P. Et Al. 2019. Studi Adsorpsi Zat Warna Naphthol Yellow Spada Limbah Cair Menggunakan Karbon Aktif Dari Ampas Tebu. Jurnal Kimia (Journal Of Chemistry). 13 (1). 104-116. https://doi.org/10.24843/JCHEM.2019.v13.i01.p16

Verayana, M.P. & H. Iyabu. 2018. Pengaruh Aktivator Hcl Dan H3PO4 Terhadap Karakteristik (Morfologi Pori) Arang Aktif Tempurung Kelapa Serta Uji Adsorpsi Pada Logam Timbal (Pb). Jurnal Entropi. 13 (1). 67-75.

Witno, W., Y. Yumna & H. S. Baso. 2024. Pengolahan Limbah Ampas Sagu Sebagai Pakan Ikan Oleh Kelompok POKDAKAN Bamba Di Desa Walenrang. Jurnal Pengabdian Pada Masyarakat. 9 (1). 79-91. https://doi.org/10.30653/jppm.v9i1.635

Jurnal Ilmiah Berkala: Sains dan Terapan Kimia
Vol. 19 No. 1, Januari 2025

Ethanol Extract of Areca Nut *(Areca catechu* L.) as a Complexing Agent to Determinate Fe(III) in Aqueous Medium

Ekstrak Etanol Buah Biji Pinang *(Areca catechu* L.) Sebagai Agen Pengompleks Untuk Penentuan Fe(III) Dalam Media Air

Pius Dore Ola[1,3*], Dodi Darmakusumah[1,2,3], Luther Kadang[1,2,3], Suwari[1,2,3], Tabita Rihi[1] and Yustina Menge Tibo[1]

[1]Department of Chemistry, Faculty of Science and Engineering/Nusa Cendana University, Kupang-85118, (NTT) Indonesia

[2]Integrated Research Center Laboratory (Biosains), Nusa Cendana University, Kupang-85118, (NTT) Indonesia

[3]Center for Research and Scipreneur of Dry Land and Archipelagic Chemistry, Nusa Cendana University, Kupang-85118, Indonesia

*Email: pius_ola@staf.undana.ac.id

ABSTRACT

A complexing agent is very critical in the analysis of metal ions with spectrophotometry UV-Vis method. The most widely used complexing agents are not eco-friendly and expensive industrial products. This work employed the ethanol extract of the areca nut as a complexing agent to determine the Fe(III) in water media, which is the most likely to pollute the environment. We found that the optimum reaction between areca nut extract with Fe(III) occurred at pH 5 and in the ratio of 21.6 mg/L Fe(III): 10 mg/L of extract. This mixture reached the highest absorbance at around 30 minutes. The spectrometric and digital image methods show the linear relation between Fe(III) concentration and absorbance with a correlation coefficient of 0.998 and 0.997 (for the green component), respectively. However, the spectrometric method shows more comparable performance parameters with the use of KSCN as a complexing agent than the digital image method using a camera (13MP) of a smartphone (Vivo V20S). This method was also applied to analyze Fe(III) in real water samples, with recovery rates ranging from 84.83% to 105.87%, all of which were deemed acceptable.
Keywords: Areca nut; complexon agent; Fe(III); Digital Image; UV-Vis Spectrophotometry; KSCN.

ABSTRAK

Agen pengompleks sangat penting dalam analisis ion logam dengan metode spektrofotometri UV-Vis. Pengompleks yang paling banyak digunakan adalah produk industri yang tidak ramah lingkungan dan mahal. Penelitian ini menggunakan ekstrak etanol biji pinang sebagai agen pengompleks untuk penentuan Fe(III) dalam media air yang merupakan pencemar lingkungan. Hasil penelitian menunjukkan bahwa kondisi optimum reaksi antara ekstrak dengan Fe(III) terjadi pada pH 5 dengan rasio 21,6 mg/L Fe(III) : 10 mg/L ekstrak. Campuran ini memiliki absorbansi paling tinggi pada pada menit ke ±30. Baik metode spektrofofometri maupun pencitraan digital memperlihatkan hubungan yang linear antara konsentrasi Fe(III) dengan absorbansi, dengan nilai koefisien korelasi berturut-turut 0.998 and 0.997. Namun demikian metode metode spektrofotometri memperlihatkan kinerja yang lebih baik dengan menggunakan KSCN sebagai pengompleks dibandingkan dengan metode pencitraan digital menggunakan kamera (13 MP) sebuah smartphone Vivo V20S. Metode ini juga diaplikasikan untuk analisis Fe(III) dalam sampel air alam, dengan nilai perolehan kembali yang berkisar antara 84,83% hingga 105,87%, yang semuanya dapat diterima.

Kata kunci: biji pinang; Agen pengompleks; Fe(III); Pencitraan digital; Spectrophotometri UV-Vis; KSCN.

Received: 04 October 2023; **Accepted**: 30 December 2024: **Available online**: 30 January 2025

1. INTRODUCTION

Iron (Fe) is one of the most widely used metals in the world, causing this metal to most likely pollute the environment, especially water. Even though iron is an essential nutrient required for various biochemical and physiological functions, its excess existence in the human body can cause health problems [Jaishankar et al., 2014], such as upset stomach, constipation, nausea, abdominal pain, vomiting, and diarrhoea [Rahmana et al., 2020]. Therefore the efforts to routinely monitor the iron level in the aqueous media are of great importance. A spectrometric method based on forming a chelate complex between Fe(III) and a complexing agent is an established method for determining Fe(III). The well-known complexing agents for Fe(III) include thiocyanate, 1, 10-phenanthroline, 2, 2'-bipyridal, bathophenanthroline, sulfosalicylic acid, and thioglycolic acid [Chen and Deng, 2021]. However, all the complexing agents mentioned are industrial products that are expensive and not eco-friendly. Therefore it is critical to seek an inexpensive and environmentally friendly complexing agent to substitute the manufactured by the chemical industry. The candidate for this purpose should be from a natural product. In this work, ethanol extract of areca nut (*Areca catechu* L.) was applied as a complexing agent to analyse Fe(III) from aqueous media.

Areca nut or betel nut is commonly referred to the seed of areca palm tree which is cultivated in South and Southeast Asian countries [Xiao et al., 2019]. The chemical composition of areca nuts, such as alkaloids, flavonoids, tannins, triterpenes, fatty acids, etc., with the tannin and flavonoids as the major components [Xiao et al., 2019]. This chemical composition benefits the medical field that is employed as an anti-bacterial, antiviral and anti-tumour, anti-oxidation, anthelmintic action, effects on the nervous system and digestive systems [Xiao et al., 2019, Fu and Chen, 2019]. In addition, due to the tannin and flavonoids contained, the extract of areca nut can also be employed as a complexing agent for analysing Fe(III). It is because structurally, tannin and flavonoids abundantly pose –OH groups, which have two lone pair electrons that can be donated to the empty orbital of Fe(III). Several works have proven the formation of the complex between tannin [Ju et al., 2017, Kraal et al., 2006, Çakar and Özacara, 2016, Selvaraj et al., 2014] and flavonoids [Kasprzak, et al., 2015, Symonowicz and Kolanek, 2012, Iqbal et al., 2015]. Therefore, ethanol extract of areca nut hypothetically can form a complex with Fe(III), and consequently can be a basis for Fe(III) analysis. Among the various extraction methods reported, ethanol solvent extraction is the most commonly employed technique. This is partly because ethanol is comparatively less toxic than acetone and methanol [Chen et al., 2020]. Additionally, ethanol as a solvent has a greater ability to extract total phenols and total flavonoids (361.22±0.26 mg GAE/g and 42.46±0.15 mg QE/g, respectively) compared to water (267.61±0.13 mg GAE/g and 16.22±0.21 mg QE/g, respectively). Both of these compounds are targeted due to their ability to form complexes with metal ions [Prayitno and Rahim, 2020]. In this work, analysis of Fe(III) was conducted in two methods that were spectrophotometric and digital image methods. In addition, the spectrophotometric method with potassium thiocyanate as a complexing agent was used as a reference.

2. MATERIALS AND METHODS

2.1. Materials

The seed of the areca nut was obtained from Timor Tengah Selatan districts, Indonesia. The ethanol extract was obtained by mixing 50 g small pieces of areca nut with 250 mL of Ethanol (technical grade, ± 70%) at room temperature for 24 h. Then, the mixture was filtered, and the filtrate was evaporated using a rotary evaporator at 70 ^{o}C for 5 h. The obtained thick extract was tested for its secondary metabolite content following the procedure reported by Iqbal [Iqbal et al., 2015] such as shown in Table 1. Nitric acid (HNO_3), Sodium acetate (CH_3COONa), and acetic acid (CH_3COOH) used to prepare the buffer solution, $FeCl_3.6H_2O$, and potassium thiocyanate (KSCN) were purchased from Merck in pro analytic grade.

Table 1. Preliminary phytochemical screening of areca nut ethanol extract

Metabolites tested	Reagent used	Observation	Result
Tannin	$FeCl_3$	Blackish blue color	+
Flavonoids	Mg + concentrate HCl	Brown precipitate formed	+
Alkaloids	Wagner	Brick red color	+
Saponins	Aquades-HCl pekat	Not frothy	-
Terpenoids	Lieberman-Burchard	Brown-red	+

2.2. Determination of optimum condition

From the theoretical consideration, it is expected that a complex compound would be formed between tannin and flavonoid in the extract with Fe(III). Therefore, it is necessary to find the optimum conditions for forming a complex compound, including pH, ratio, and stable time. The determination of those parameters was conducted by modifying the procedure proposed by Liu [Liu et al., 2011], as follows: 2.5 mL of tannin 100 mg/L (dissolved in methanol 50 %) and 21.5 mL of acetate buffer solution (prepared by mixing of a certain volume of nitric acid 0.1 mol/L, acetic acid 0.1 mol/L and sodium acetate 0.1 mol/L), were mixed. Into the mixture, 1.0 mL of Fe(III) salt of 1.0 mmol/L (dissolved in HCl 0.1 mol/L) was added and the absorbance of the mixture was measured.

2.3. Determination of analytical performance parameters

A series of Fe(III) standard solutions was prepared based on the obtained optimum conditions. Each standard solution absorbance was obtained using spectrophotometric and digital image methods. In the case of the digital image technique, the measurement procedure was conducted by placing each standard solution in the bottom centre of the styrofoam box. This styrofoam box (20 x 20 x 20 cm) with a window (4 x 4 cm) was equipped with a 30-watt Visicom LED bulb lamp (**Fig. 1**) to maintain the same environmental light condition during image recording. Through the box window, the picture was captured using a camera (13 MP) of a smartphone (Vivo V20S) at a distance of 9 cm between the camera and the sample. The RGB viewer software installed in the computer was used to image the pictures as colour intensities of Red, Green and Blue (RGB), which were then converted to absorbance using the Lambert-Beer equation. A calibration curve was constructed using the obtained absorbance, where several analytical performance parameters can be evaluated. While the two other analytical performance parameters, viz precision and accuracy, can be estimated by repeated measurement of six standard solutions of Fe(III) with a certain concentration. As a reference method, a spectrophotometry UV-Vis with KSCN as a complexing agent has also been employed in calibration curve construction and precision and accuracy estimation.

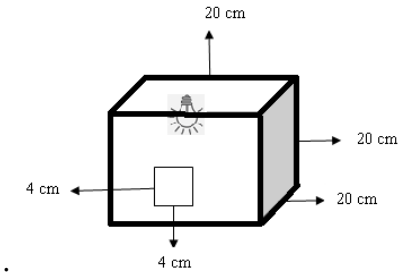

Figure 1. Styrofoam box for taking photos of samples

3. RESULTS AND DISCUSSION

3.1. Determination of optimum condition

Based on the preliminary phytochemical screening test, the ethanol extract of the areca nut contains both tannin and flavonoid (Table 1). These metabolites potentially react with metal ions due to their ability to donate their lone pair electron to the un occupation orbital of the metal ion. Therefore, the optimum condition for the reaction between extract and Fe(III), including pH, ratio, and stability time, should be found first. The result of optimation is shown in the **Fig. 2**.

An amount of 0.5 mL Fe(III) 270 mg/L and 0.5 mL of extract 100 mg/L were mixed, and the mixture was then diluted with various pH of acetate buffer to figure the effect of pH on the reaction between Fe(III) with the extract. The absorbance of the mixture at 531 nm is shown in Figure 2(a). This result shows that the highest absorbance was observed at pH 5, which means that the highest concentration of Fe(III)-extract was formed at this pH. At the lower and the higher pH, the presence of H^+ and OH^- probably disturbed the stability of the complex. This optimum pH was then used to search the ratio between Fe(III) and the extract. The different volumes of Fe(III) 270 mg/L and 0.5 mL of extract 100 mg/l were mixed and diluted with acetate buffer pH 5. The absorbance of each mixture at 531 nm was recorded and displayed in Figure 2(b). Figure 2(b) shows that the highest concentration of Fe(III)-extract was achieved when 0.4 mL of Fe(III) 270 mg/L was added to 0.5 mL of extract 100 mg/L. The optimum pH and ratio were then applied to evaluate the mixture's stable time, as indicated in Figure 2(c). This result implies that the best measurement was around 30 minutes after mixing.

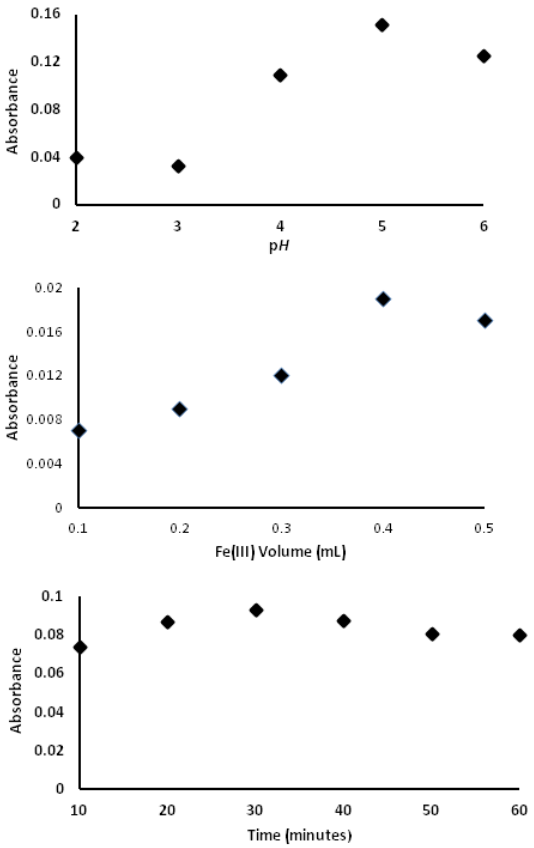

Figure 2. Optimum pH (a), ratio (b), and the stable time (c) for the reaction between Fe(III) and extract

3.2. Standard curve preparation and analytical performance parameters determination

Based on the result in **Fig. 2(b)**, 21.6 mg/L Fe(III) needed 10 mg/L of extract to form a mixture with the highest absorbance. Considering this result, the extract concentration needed to prepare the Fe(III) standard solution with concentrations of 2, 4, 6, 8, and 10 mg/L were around 5 mg/L. Fe(III) and extract concentrations mentioned were the concentration after diluting with buffer pH 5,

which also served as a blank solution. Those standard solutions were then recorded their absorbance with a spectrophotometer UV-Vis, and the result is presented in **Fig. 3**.

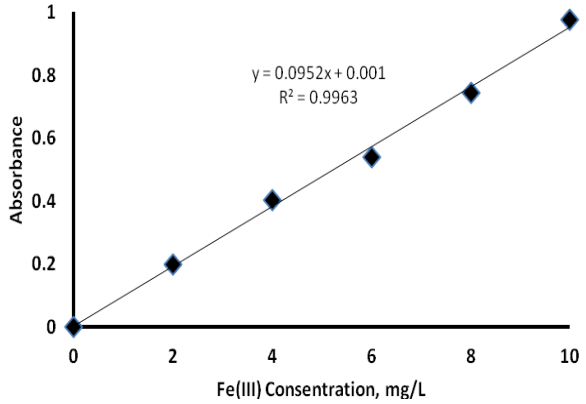

Figure 3. Standard curve of a spectrometric method with extract as a complexing agent

The correlation coefficient (r) of 0.998 indicated that the ethanol extract of the areca nut could be utilized as a complexing agent to determine the Fe(III) concentration from the aqueous media. In addition, the absorbance of those standard solutions was also obtained from imaging pictures using RGB viewer obtained by digital image method using a styrofoam box (Figure 1), as shown in **Fig. 4**.

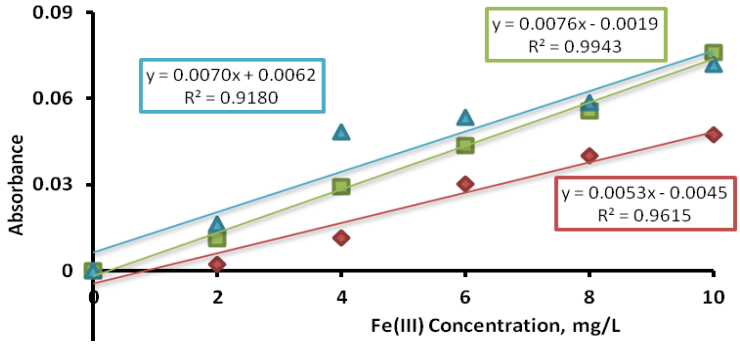

Figure 4. Standard curve of a digital image method with extract as a complexing agent

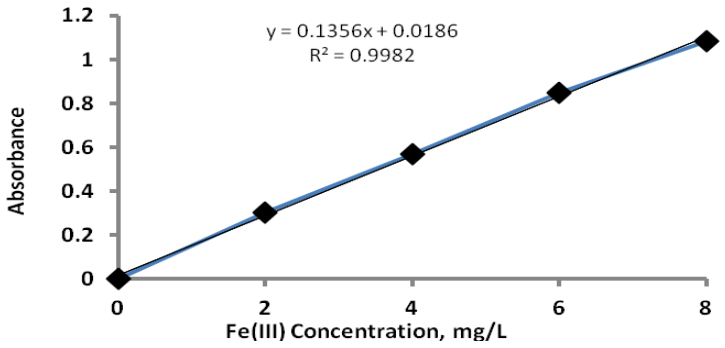

Figure 5. Standard curve of a spectrometric method with KSCN as a complexing agent

Fig. 4 shows that the ethanol extract of the areca nut can also be employed as a complexing agent using the digital image method. The green component indicated the straightest line (r= 0.997), and the green colour was employed in the further experiment. As a

reference, Fe(III) standard curve was also constructed using spectrometric method with KSCN as a complexing agent as presented in **Fig. 5**.

The two other analytical performance parameters, viz precision and accuracy, were estimated by repeating measurement concentration of six standard solutions of Fe(III) 8 mg/L, as denoted in Table 2.

Data in Table 2 was employed to calculate the t and f, which was then used to estimate the method's accuracy and precision by comparing them with the t and f table at a certain confidence level. Assisted by **Fig. 3, Fig. 4, Fig. 5,** and Table 2, the analytical performance parameters could be evaluated as represented in Table 3.

Table 2. Measured concentration of Fe(III) 8 mg/L

Repetition	Measured Fe(III) concentration, mg/L		
	Spectrophotometric, KSCN as complexing	Spectrophotometric, extract as complexing	Digital image, extract as complexing
1	7.881	7.839	7.907
2	7.859	7.844	7.578
3	7.874	7.857	7.907
4	7.866	7.849	7.907
5	7.903	7.895	7.578
6	7.888	7.891	7.907
Average	7.8785	7.8625	7.7973
SD	0.016	0.024	0.170

Table 3. Determination of several analytical performance parameters in comparison with the spectrometric method with KSCN as a complexing agent

Parameters	Result		
	S-KSCN	S-Extract	DI-Extract
Error (%)	1.513	1.719	2.538
Precision (%RSD)	0.203	0.305	2.180
LoD, (mg/L)	0.354	0.756	67.105
LoQ, (mg/L)	1.180	2.321	223.684
Sensitivity	0.1356	0.0952	0.0076
t_{count}	1.358	$t_{count} < t_{table}$	1.165	$t_{count} < t_{table}$
t_{table} ($\alpha = 0{,}05$)	2.228	Not significantly different	2.228	Not significantly different
f_{count}	2.250	$f_{count} < f_{table}$ Not significantly different	112.891	$f_{count} > f_{table}$ Significantly different

S-KSCN: spectrometric method with KSCN as a complexing agent; **S-Extract**: spectrometric method with ethanol extract of areca nut as a complexing agent; **DI-Extract**: digital image method with ethanol extract of areca nut as a complexing agent.

Data on the Tabel 3 indicate that the precision of the digital image method with extract of areca nut as a complexing agent was significantly different with a reference method, namely the spectrometric method with KSCN as a complexing agent. It is exacerbated by a very high detection limit (LoD). Therefore, this method is not suitable for analyzing samples of water that generally have low Fe(III) concentrations, typically measured in part per milion or even part per bilion units. On the other hand, the spectrometric method with an extract of areca nut as a complexing agent denotes better performance. The accuracy and precision of this method were like the reference method.

The LoD of this method was also far lower than the digital image method. Therefore the spectrometric method with areca nut extract as a complexing agent was applied to analyse Fe(III) from the real sample of water.

3.3. Application of the method to the real sample of water

The applicability of this method to analyze Fe(III) has been verified to two kinds of samples, namely well water and tap water. A little hydrogen peroxide was added to each sample to oxidize Fe(II), which may be present in the sample to Fe(III). Firstly, the concentration of Fe(III) in the sample was determined using the spectrometric method with KSCN as a complexing agent. Due to the very low Fe(III) concentration in the real water sample, an amount standard of Fe(III) was added so that its concentration became higher than LoD. Adding the ethanol extract of the areca nut to the sample was carried out according to the optimum ratio. The mixture was then diluted with an acetate buffer of pH 5. The absorbance was recorded, and the recovery is shown in Table 4.

Table 4. Recovery of Fe(III) in the real sample of water using the spectrometric method with areca nut extract as a complexing agent

Samples	p*H*	Fe(III) Concentration (mg/L)			Recovery (%)
		Initial*	added	measured	
Well water	6.15	0.006	0.6	0.528	87.60
			0.8	0.681	84.83
Tap water	6.97	0.007	0.6	0.637	105.70
			0.8	0.801	99.78

* Initial concentrations of 0.006 and 0.007 mg/L were in 4 mL of samples. Because of diluting to 10 mL, the initial concentration changed to 0.0024 and 0.0028 mg/L, respectively.

The result in Table 4 indicates that the measurement recoveries are in the range of acceptable. According to Latimer et al. (2023), the acceptable %R for an analyte concentration of 0.1% ranges from 80% to 110%. It means that the ethanol extract of areca nut could be a complexing agent candidate for Fe(III) analysing using the spectrometry method.

4. CONCLUSIONS

In this work, ethanol extract of areca nut was employed as a complexing agent in analysing Fe(III) from water media. The optimum reaction condition between extract and Fe(III) occurred at pH 5 and in the ratio of 21.6 mg/L Fe(III): 10 mg/L of extract. The highest absorbance was observed at around 30 minutes. The spectrometric method with extract as a complexing agent shows comparable analytical performance parameters (%E: 1.719; %RSD: 0.305; LoD: 0.756; LoQ: 2.321; and Sensitivity: 0.0952) with using KSCN as a complexing agent (%E: 1.513; %RSD: 0.203; LoD: 0.354; LoQ: 1.180; and Sensitivity: 0.1356). Applying this method to determinate Fe(III) in the real water sample indicates that the recovery of all samples experimented were in range of acceptable.

LIST OF REFERENCES

Çakar, S., and Özacara, M. (2016). Fe-Tannic Acid Complex Dye as Photo Sensitizer for Different Morphological ZnO Based DSSCs. *Spectrochim. Acta A Mol. Biomol. Spectrosc*. *163*, 79-88. https://doi.org/10.1016/j.saa.2016.03.031.

Chen, H., Xiao, H., and Pang, J. (2020). Parameter Optimization and Potential Bioactivity Evaluation of a Betulin Extract from White Birch Bark. *Plants 9*, 392. doi:10.3390/plants9030392).

Chen, X., He, Y., and Deng, Y. (2021). Chemical Composition, Pharmacological, and Toxicological Effects of Betel Nut. *Evid.*

Based Complementary Altern. Med. *2021:* 1-7. https://doi.org/10.1155/2021/1808081.

Fu, Z., and Chen, R. (2019). Study of Complexes of Tannic Acid with Fe(III) and Fe(II). *J. Anal. Methods Chem*. *2019*, 1-6. https://doi.org/10.1155/2019/3894571.

Iqbal, E., Salim, K. A., and Lim, L.B.L. (2015). Phytochemical Screening, Total Phenolics and Antioxidant Activities of Bark and Leaf Extracts of Goniothalamus Velutinus (Airy Shaw) from Brunei Darussalam. *J. King Saud Univ. Sci*. *27*(3), 224-232. https://doi.org/10.1016/j.jksus.2015.02.003.

Jaishankar, M., Tseten, T., Anbalangan, N., Methew,B. B., and Beeregowda, K. N. (2014). Toxicity, Mechanism and Health Effects of Some Heavy Metals. *Interdiscip Toxicol*. ; ***7*** (2), 60-72. https://pubmed.ncbi.nlm.nih.gov/26109881/.

Ju, S.-W., Prajatelistia, E., Jun, S. H., Hwang, D.S., Ahn, J.-S., and Sanandiya, N. D. (2017). Aesthetically Improved and Efficient Tannin–Metal Chelates for the Treatment of Dentinal Hypersensitivity. *RSC Adv*., ***7***(87), 87-94. DOI: 10.1039/c6ra24745h.

Kasprzak, M. M., Erxlebenc, A., and Ochocki, J. (2015). Properties and Applications of Flavonoid Metal Complexes. *RSC Adv.***,** *5*: 45853-45877. https://doi.org/10.1039/C5RA05069C

Kraal, P., Jansen, B., Nierop, K. G., and Verstraten, J. M. (2006). Copper Complexation by Tannic Acid in Aqueous Solution. *Chemosphere 65*(11), 2193-2198. https://doi.org/10.1016/j.chemosphere.2006.05.058.

Latimer, G. W., Horwitz, W., and AOAC International (Eds.). (2023). *Official methods of analysis of AOAC International: OMA* (22nd edition). Oxford New York, NY: AOAC International. https://doi.org/10.1093/9780197610145.001.0001

Liu, R., Tindall, S. R., Hagerman, A. E., Gonzales, J. M., and Halvorson, J. J. (2011) Characterization of Tannin-Metal Complexes by UV-Visible Spectrophotometry. *National Meeting and Exposition of the* American *Chemical Society 241*.

Prayitno, S.A., and Rahim, A. R. (2020). Comparison of Extracts (Ethanol And Aquos Solvents) Muntingia calabura Leaves on Total Phenol, Flavonid And Antioxidant (Ic50) Properties. *KONTRIBUSIA, 3(2)*, 319-325.

Rahmana, K. M., Biswasa, B., Neger, T., Sharmina, N., and Rahman, L. (2020). Method Validation on Iron Determination by Spectrophotometric Method in Aqueous Medium. *Indian J. Chem. 59A*, 790-796. http://op.niscair.res.in/index.php/IJCA/article/view/23672

Selvaraj, S., Krishnaswamy, S., Devashya, V., Sethuraman, S., and Krishnan, U. M. (2014). Flavonoid-Metal Ion Complexes: a Novel Class of Therapeutic Agents. *Med Res Rev*.*34*(4), 677-702. doi: 10.1002/med.21301.

Symonowicz, M., and Kolanek, M. (2012). Flavonoids and Their Properties to Form Chelate Complexes. *Biotechnol Food Sci*. *76* (1), 35-41. https://core.ac.uk/download/pdf/53096166.pdf

Xiao, Y., Yang, Y., Yong, J. and Lu, C. (2019). Chemical Components and Biological Activities of Areca catechu L. *Biomed Res Rev*, 3, 1- 4. 10.15761/BRR.1000131.